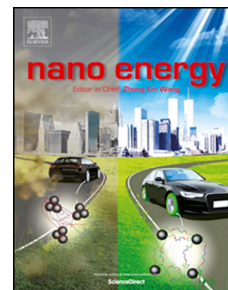


# Journal Pre-proof

Re-usable self-poled piezoelectric/piezocatalytic films with exceptional energy harvesting and water remediation capability

Biswajoy Bagchi, Nur Amin Hoque, Norbert Janowicz, Sukhen Das, Manish K. Tiwari



PII: S2211-2855(20)30916-2

DOI: <https://doi.org/10.1016/j.nanoen.2020.105339>

Reference: NANOEN 105339

To appear in: *Nano Energy*

Received Date: 4 May 2020

Revised Date: 16 August 2020

Accepted Date: 28 August 2020

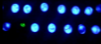
Please cite this article as: B. Bagchi, N.A. Hoque, N. Janowicz, S. Das, M.K. Tiwari, Re-usable self-poled piezoelectric/piezocatalytic films with exceptional energy harvesting and water remediation capability, *Nano Energy* (2020), doi: <https://doi.org/10.1016/j.nanoen.2020.105339>.

This is a PDF file of an article that has undergone enhancements after acceptance, such as the addition of a cover page and metadata, and formatting for readability, but it is not yet the definitive version of record. This version will undergo additional copyediting, typesetting and review before it is published in its final form, but we are providing this version to give early visibility of the article. Please note that, during the production process, errors may be discovered which could affect the content, and all legal disclaimers that apply to the journal pertain.

© 2020 Published by Elsevier Ltd.

**Credit Author Statement**

**Biswajoy Bagchi:** Joint Conceptualization, Visualization, Methodology, Formal analysis, Investigation, Writing- Original draft, Writing-Review and Editing. **Nur Amin Hoque:** Methodology, Validation, Formal analysis. **Norbert Janowicz:** Methodology, **Sukhen Das:** Resources, **Manish K Tiwari:** Joint Conceptualization and Supervision, Visualization, Project management, Formal analysis, Validation, Resources, Funding Acquisition, Writing-Review and Editing.



Energy  
harvesting

Dye  
degradation



**MoS<sub>2</sub>-PVDF**



## Re-usable self-poled piezoelectric/piezocatalytic films with exceptional energy harvesting and water remediation capability

Biswajoy Bagchi<sup>1,2</sup>, Nur Amin Hoque<sup>3</sup>, Norbert Janowicz<sup>2</sup>, Sukhen Das<sup>3</sup>, Manish K. Tiwari<sup>\*1,2</sup>

<sup>1</sup>Wellcome/EPSRC Centre for Interventional and Surgical Sciences (WEISS), University College London, London, W1W 7TS, UK

<sup>2</sup>Nanoengineered Systems Laboratory, UCL Mechanical Engineering, University College London, London, WC1E 7JE, UK

<sup>3</sup>Jadavpur University, Department of Physics, Kolkata, 700032, India

\*Corresponding author

E-mail: [m.tiwari@ucl.ac.uk](mailto:m.tiwari@ucl.ac.uk), Contact: +442031081056

### Abstract

The need for sustainable technologies to address environmental pollution and energy crisis is paramount. Here we present a novel multifunctional nanocomposite, free standing films by combining piezoelectric molybdenum sulphide (MoS<sub>2</sub>) nanoflower with poly vinylidene fluoride (PVDF) polymer, which can harness otherwise wasted mechanical energy for useful energy generation or water purification. The unique MoS<sub>2</sub> nanoflower morphology is exploited to render the whole nanocomposite piezo active. A number of features are demonstrated to establish potential practical usage. Firstly, the nanocomposite is piezoelectric and piezocatalytic simultaneously without requiring any poling step (i.e. self-poled). Secondly, the self-poled piezoelectricity is exploited to make a nanogenerator to produce electrical power. The nanogenerator produced >80 V under human finger tapping with a remarkable power density, reaching 47.14 mW cm<sup>-3</sup>. The nanocomposite film is made by simple solution casting, and the corresponding nanogenerator powers up 25 commercial LEDs by finger tapping. Last but not the least, the developed films show efficient, fast and stable piezocatalytic dye degradation efficiency (>90% within 20 minutes) against four different toxic and carcinogenic dyes under dark condition using only ultrasonic vibration. Reusability of at least 10 times is also demonstrated without any loss of catalytic activity. Overall, our nanocomposite has clear potential for use as self-powered sensor and energy harvester, and in water remediation systems. It should potentially also be deployable as a surface mounted film/coating in process engineering, industrial effluent management and healthcare devices systems.

**Keywords:** MoS<sub>2</sub> nanoflower; PVDF; self-poling; nanogenerator; piezocatalysis; water remediation

## Introduction

Bioaccumulation of emerging inorganic and organic contaminants such as toxic dyes, pharmaceuticals, and drugs in wastewater effluents, natural environment and drinking waters has grown at an alarming rate in recent times and presents a huge challenge for water reuse industry [1,2]. Water pollutants such as common pesticides, herbicides, organic dyes and biological contaminants such as DNA, proteins, lipids, bacteria, virus, spores etc., present a serious and persistent threat to human health. This has prompted the development of some advanced disinfection and water remediation techniques which involves reactive oxygen species (ROS). ROS consisting of a medley of strong oxidizing agents like OH•, H•, O•, O<sub>3</sub>, H<sub>2</sub>O<sub>2</sub> etc. that can safely and effectively destroy a large number non-living and living organic contaminants in water. Among the contaminants, organic dyes are particularly challenging to decontaminate since most dyes used in textile, pharmaceutical, food industries and agriculture are not only toxic to the environment but also tend to be potentially carcinogenic. Thus, complete breakdown and/or removal of these contaminants in industry effluents as well as drinking water is absolutely essential for long term benefit to human health and environment [2-5]; and doing so in a safe and energy-efficient manner is a major scientific challenge. Current ROS based water treatment technologies such as UV photolysis, radiolysis, ozonation, sonochemistry, electrical discharge technology, electron-beam irradiation and supercritical water oxidation require expensive set up and continuous energy source in the form of electricity or ultraviolet light source [4, 6-7]. Although, photocatalysis has shown promise but is limited by agglomeration tendency, post-separation difficulty and low efficiency under solar irradiation<sup>8</sup>. Here we present a *passive* (i.e. without requiring any additional energy input), effective, cheap and eco-friendly processes for ROS mediated disinfection and degradation of dyes using a novel piezocatalytic nanocomposite. As an additional benefit, we also demonstrate the ability of our nanocomposite to serve as a nanogenerator for energy-harvesting applications, thereby offering a promise for self-powered sensing and optoelectronic devices.

Piezoelectric materials can produce electric charge when subjected to mechanical stress and vice-versa [8, 9]. Mechanically straining a piezoelectric material induces an electric field throughout the material which generates free charges at its interface with the ambient (e.g. air or water). Piezocatalytic materials are a subclass of piezoelectric materials, where the

material composition is engineered such that the free charges in turn generate several reactive oxygen species (ROS) including  $\cdot\text{OH}$ ,  $\cdot\text{O}^-$ ,  $\cdot\text{HO}_2$  and  $\text{H}_2\text{O}_2$  by local micro-electrolysis of water. The ROS generated by mechanical actuation of piezoelectric materials thus can be efficiently used to piezocatalytically oxidize and degrade the toxic and/or carcinogenic dyes and microbes in water from textile, chemical, pharmaceutical and food industries [10-14].

These piezoelectric materials can also be activated when subject to ambient vibrations which are abundant in daily life. For example, piezoelectric ceramics in the form of ZnO and Cu/ZnO nanowires,  $\text{Pb}(\text{Zr}_{0.52}\text{Ti}_{0.43})\text{O}_3$  fibers,  $\text{ZnSnO}_3$  nanowires, single/few-layers  $\text{MoS}_2$  nanoflowers and nano/micrometer sized  $\text{BaTiO}_3$ , etc. have all been reported to piezocatalytically degrade potentially harmful dyes e.g. Acid Orange 7, Rhodamine B, Methyl Orange, 4-chlorophenol under ultrasound vibrations with high efficiency [11, 15-21]. Thus, harnessing the abundant vibrational and otherwise wasted mechanical energy to piezocatalytically treat waste-water can truly boost water purification technology in an energy-efficient manner. However, using free piezoelectric nanoparticles directly in water treatment presents several problems in the form of stability of the nanoparticles, efficacy, accumulation, toxicity, separation and recyclability. Here we propose a flexible, polymer nanocomposite film as an alternative solution to overcome these limitations. Our hybrid piezoelectric films are based on PVDF and  $\text{MoS}_2$  nanoflowers, which can be processed simply through solution processing and demonstrate excellent piezoelectric properties without requiring energy intensive poling – our nanocomposites are self-poled. The mechanism of self-poling is discussed in detail and the functionality is established by demonstrating that our films can also be used in energy-harvesting applications, such as the so called nanogenerators for self-powered sensing systems [22]. To demonstrate the dual-use feature, our hybrid nanocomposite films are shown to exploit vibration induced electromechanical coupling to promote remarkable energy harvesting capability (demonstrated by fabricating nanogenerator device which is able to power up LEDs by human finger tapping) as well as catalytic degradation of potentially toxic and carcinogenic dyes like, Acridine Orange [23], Eosin Y [24], Ethidium Bromide [25] and Rhodamine B [26].

The piezocatalytic activity in  $\text{MoS}_2$  nanoflowers was first reported by Wu *et al.* [11], who showed ultrafast degradation of Rhodamine B in water under dark condition. However, for practical application, the process runs the risk of contaminating water with  $\text{MoS}_2$  nanoparticles itself. Further, it is not suitable for treating flowing water due to loss of

nanoparticles over time. Thus, a self-sustained system whereby the MoS<sub>2</sub> nanoflowers are held stationary is required for long term application. PVDF polymer has been well known for its robustness, chemical inertness and piezoelectricity, which therefore would be an ideal candidate to act as a substrate for arresting MoS<sub>2</sub> nanoflowers. Currently, MoS<sub>2</sub>-PVDF based nanocomposites reported so far mainly focusses on energy harvesting applications rather than dye degradation, for example, Cai *et al.* [27], studied mainly MoS<sub>2</sub> nanosheet induced  $\beta$  phase transformation and mechanical aspects of PVDF films. Maity *et al.* [28], showed nanogenerator and sensing performance with salt exfoliated bulk MoS<sub>2</sub> and electrospun PVDF composite. Similarly, Sahatiya *et al.* [29], used electrospun PVDF and MoS<sub>2</sub>-cellulose for hybrid piezo-triboelectric nanogenerator. However, in both the applications, electrically poled PVDF nanofibers were used and no piezocatalytic properties were reported.

In the current work we are introducing a number of new features. For the first time, we are introducing a self-poled, deployable MoS<sub>2</sub> nanoflower doped PVDF film, which demonstrates excellent piezoelectric (through an energy harvesting nanogenerator) and piezocatalytic functions. The unique strategy of combining MoS<sub>2</sub> nanoflowers in PVDF matrix results in a multifunctional, robust, nontoxic and flexible film where the enhanced piezoelectricity is achieved by synergistic interaction between MoS<sub>2</sub> and PVDF without requiring any high voltage poling process [28,30] while the piezocatalytic effect is observed due to vibration induced ROS generation at the water/film interface. The nanogenerator developed using our self-poled MoS<sub>2</sub>-PVDF film exhibited much superior performance compared to similar nanocomposites and repeatable multi-dye degradation capability showing versatility. The simple solution casting approach to nanocomposite film synthesis is scalable and economical, and the embedded MoS<sub>2</sub> nanoparticles offer the potential for long term activity, recyclability and the ability to treat large volumes of water without any risk of nanoparticle spillage. Additionally, use of a nanocomposite film instead of simply using the MoS<sub>2</sub> nanoflower for piezocatalytic water remediation means that there will be no need to remove the nanoparticles. Therefore, PVDF and MoS<sub>2</sub> nanoflower have a complementary role in the reported nanocomposite functionality. Notably, our approach is different from recent work by Lin *et al.* [31] who blended nanoflower MoS<sub>2</sub> with poly(dimethyl siloxane) (PDMS) to obtain piezocatalytic behaviour and also used the nanocomposite to develop a *triboelectric* nanogenerator; our focus is on the self-poling, piezoelectric feature imparted to PVDF by MoS<sub>2</sub> nanoflowers. Besides the difference in mechanism, our nanocomposites also

shows superior nanogenerator power density and stable piezocatalytic activity for re-usability (>90% dye- degradation efficiency is maintained even after using the same film 10 times).

## Materials and Methods

### *Synthesis of MoS<sub>2</sub> nanoflowers*

The MoS<sub>2</sub> nanoflowers were synthesized by hydrothermal process. Typically, 0.28 g of Pluronic F-127 (Merck, Germany) was dissolved in 140 mL of distilled water. Next 8.5g of Ammonium heptamolybdatetetrahydrate, (NH<sub>4</sub>)<sub>6</sub>Mo<sub>7</sub>O<sub>24</sub>·4H<sub>2</sub>O, (Merck, Germany) and 1.28 mg Thiourea, CH<sub>4</sub>N<sub>2</sub>S, (Merck, Germany) were added to the solution and allowed to stir at room temperature for 30 min. The resulting homogeneous solution was then loaded in a stainless-steel Teflon lined hydrothermal reactor and was kept in an oven at 200°C for 24 h [12]. After the reaction, the black precipitate was centrifuged and washed with water and alcohol repeatedly. The precipitate was then dried to get a free-flowing powder and stored for further characterization and use.

### *Synthesis of MoS<sub>2</sub>-PVDF films*

MoS<sub>2</sub> nanoflower doped PVDF film was fabricated using solution processing. Initially, 250 mg of PVDF (Sigma-Aldrich, Germany; Mw: 180,000 GPC; Mn: 71000) was dissolved in 60 mL of Dimethyl sulfoxide (DMSO) (Merck, Germany) under constant magnetic stirring at 60°C to obtain a homogeneous solution. Next, MoS<sub>2</sub> (10 wt% of PVDF) powder was added to the PVDF solution and continuously stirred at room temperature until complete dispersion was achieved. Afterwards, the colloidal suspension was transferred to a clean petri dish and dried at 80° C in an oven to get nanocomposite films [22]. For comparison, pure PVDF film was also prepared in a similar manner without MoS<sub>2</sub>.

### *MoS<sub>2</sub>-PVDF nanogenerator (MPNG) fabrication*

As a first application of the nanocomposite, a nanogenerator was fabricated by using an MoS<sub>2</sub>-PVDF film of dimension 1 cm × 1 cm × 50 μm. A 40 μm thick copper/aluminium electrode was attached on either sides of the film and two copper wires were connected to side of the film. Next, the film containing the electrodes and connecting wires are packaged in polydimethylsiloxane (PDMS) (Sylgard 184, Dow Corning, ratio of 1:10) by immersing the nanocomposite films in PDMS gel and drying for 15 min in a vacuum followed by drying at 60 °C for 1 h to remove the bubbles from the mixture [22]. The final package size of the as-fabricated MPNG device was 2 cm × 2 cm × 0.3 cm.



### *Piezocatalysis experiment*

*MoS<sub>2</sub>-PVDF* nanocomposite film of dimension 2 cm × 2 cm and thickness 50 μm was immersed in 10 mL of 10 ppm solutions of each dye (i.e., Acridine Orange (AO), Eosin Y (EO), Ethidium Bromide (ET) and Rhodamine B (RHO) (Loba chemie) in deionised water. The conical flask containing the dye solution and the nanocomposite film was placed in a bath sonicator (RS Pro Ultrasonic Cleaner, 100W) and subjected to pulsed ultrasonic vibrations for 20 mins. During the experiment, a small portion of the dye solution was pipetted out at regular intervals (0, 5, 10, 15 and 20 min) and measured using UV-Visible spectrophotometer to check its degradation. The percent degradation and the rate constant were calculated from the measured data. A recyclability test was also performed with Rhodamine B which included 10 cycles of catalytic experiments using 200 mL of 10 ppm dye concentration to determine the efficacy of the nanocomposite films for treating large volumes of water. All the catalytic experiments were carried out in dark at 25 °C.

### *Instrumental*

Physico-chemical characteristics including phase formation, microstructure, elemental distribution and thermal properties of MoS<sub>2</sub> nanoflower and MoS<sub>2</sub>-PVDF film was performed using X-ray diffraction (XRD; Model-D8, Bruker AXS Inc., Madison, WI), Fourier transform infrared (FTIR) spectroscopy (FTIR-8400S, Shimadzu), Field emission scanning electron microscopy (FESEM; INSPECT F50, Netherlands), Energy dispersive x-ray analysis (EDAX) and Differential scanning calorimetry (DSC-60, Shimadzu). Ferroelectric properties of the film were measured in terms of polarization-electric field (P-E loop) using Hysteresis version 4.9.0 (Radiant technologies).

Open circuit voltage ( $V_{oc}$ ) generated by the MPNG under continuous finger imparting and ultrasound was measured using a digital storage oscilloscope (Keysight, Oscilloscope DSO-X 3012A). Short circuit current ( $I_{sc}$ ) was recorded under the same condition using Keysight, Electrometer B2985.

Catalytic degradation of dyes was monitored using a UV-Visible spectrophotometer (Lambda 650, Perkin Elmer) and •OH was measured with terephthalic acid (Merck, Germany) using a Cary Eclipse Fluorescence spectrophotometer (Agilent Technologies).

## **Results and Discussion**

Figure 1 shows the schematic of MoS<sub>2</sub> and MoS<sub>2</sub>-PVDF nanocomposite synthesis procedure. The synthesis procedure described is a simple, water-based technique using Pluronic F-127 as the structure directing agent.

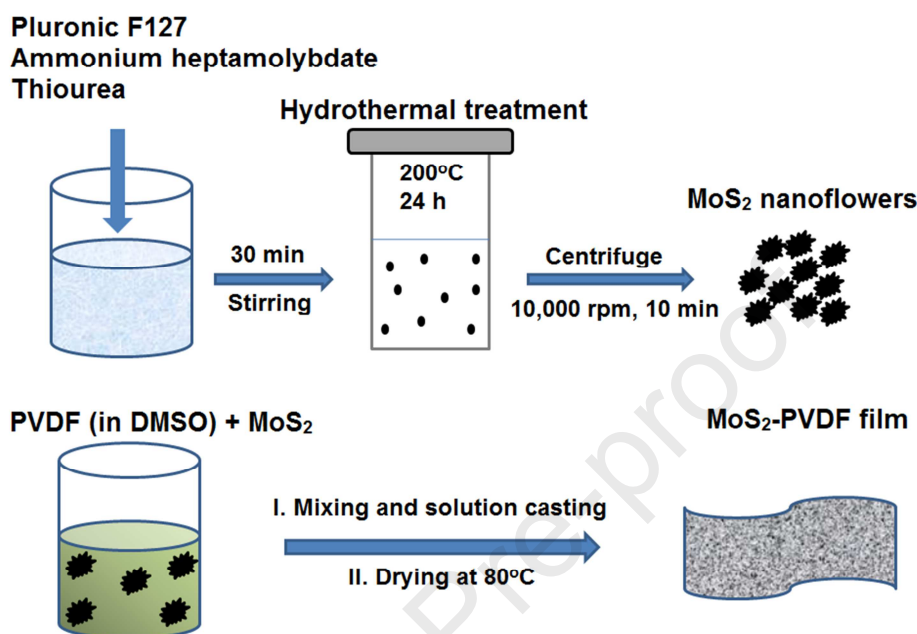


Figure 1: Scheme of MoS<sub>2</sub>-PVDF nanocomposite film preparation.

The role of F127 in promoting mesoporous flower like structure in  $\gamma$ -alumina is well documented by Ge *et al.* [32], and it is interesting to see that it also directs nanoflower morphology in case of MoS<sub>2</sub>. This provides an alternative, less expensive way than commonly used solvent like 1-Butyl-3-methylimidazolium chloride.

#### *XRD analysis*

The XRD pattern of pure MoS<sub>2</sub> and MoS<sub>2</sub>-PVDF film is represented in Figure 2a. MoS<sub>2</sub> shows characteristic broad reflections at 13.97° (002), 33.66° (102), 39.97° (103), 49.94° (105) and 59.41° (110) which confirms phase formation in the as synthesized powder [11] (JCPDS card No. 37-1492). Addition of MoS<sub>2</sub> nanoflowers significantly promotes nucleation of polar electroactive  $\beta$ -crystals in PVDF film which is indicated by a sharp single peak at  $2\theta = 20.5^\circ$  ((110), (200)) and absence of  $\alpha$  phase reflections. In addition, reflections corresponding to MoS<sub>2</sub> are also present indicating the composite nature of the film (Figure 2a). Electroactive  $\beta$  phase crystallization in PVDF is often achieved by introducing variety of molecules including ceramics, salts, clays, polymers, nanoparticles etc., whereby interfacial

interaction with the C-H and fluorine groups leads to the all *trans* TTTT conformation [22, 30, 33]. In the present case, addition of MoS<sub>2</sub> seems to be playing a similar role.

#### FTIR analysis

Comparison of FTIR spectra (Figure 2b) of the pure MoS<sub>2</sub> and the MoS<sub>2</sub>-PVDF films also indicates enhanced electroactive  $\beta$  phase formation in the composite film. Pure PVDF shows characteristic absorbance bands of nonpolar  $\alpha$ -crystals at 488 cm<sup>-1</sup> (CF<sub>2</sub> wagging), 532 cm<sup>-1</sup> (CF<sub>2</sub> bending), 615 and 764 cm<sup>-1</sup> (CF<sub>2</sub> bending and skeletal bending), and 796 and 976 cm<sup>-1</sup> (CH<sub>2</sub> rocking). A small peak at 840 cm<sup>-1</sup> (CH<sub>2</sub> rocking, CF<sub>2</sub> stretching, and skeletal C–C stretching) is also observed in the spectrum of pure PVDF, which may be due to the slight presence of  $\beta$  or  $\beta + \gamma$  crystals (Figure 2b). In case of MoS<sub>2</sub>-PVDF, all of the characteristic peaks corresponding to nonpolar  $\alpha$ -crystals are absent with absorbance bands at 445 cm<sup>-1</sup> (CF<sub>2</sub> rocking and CH<sub>2</sub> rocking), 479 cm<sup>-1</sup> (CF<sub>2</sub> deformation), 510 cm<sup>-1</sup> (CF<sub>2</sub> stretching), 600 cm<sup>-1</sup> (CF<sub>2</sub> wag), and 840 and 1274 cm<sup>-1</sup> becoming predominant. The appearance of 510 cm<sup>-1</sup> and 840 cm<sup>-1</sup> band along with 445 cm<sup>-1</sup> and 1274 cm<sup>-1</sup> bands and the absence of the characteristic absorbance band of  $\gamma$  crystals at 1234 cm<sup>-1</sup> confirms nucleation of electroactive  $\beta$ -crystals in the MoS<sub>2</sub> doped PVDF film [28,30]. Presence of MoS<sub>2</sub> was confirmed from the vibrations around 480 cm<sup>-1</sup> (Mo-S stretching), 900 cm<sup>-1</sup> (S-S stretching) and 1100 cm<sup>-1</sup> (O-H stretching) which almost merges with the PVDF bands. The fraction of electroactive  $\beta$  phase content in the nanocomposite MoS<sub>2</sub>-PVDF film was calculated by using the Lambert-Beer Law

$$F(\beta) = \frac{A_{\beta}}{\left(\frac{K_{\beta}}{K_{\alpha}}\right)A_{\alpha} + A_{\beta}}$$

where  $A_{\alpha}$  is the absorbance at 764 cm<sup>-1</sup>,  $A_{\beta}$  is the absorbance at 840 cm<sup>-1</sup> and  $K_{\beta}$  equals  $7.7 \times 10^4$  cm<sup>2</sup> mol<sup>-1</sup> and  $K_{\alpha}$  equals  $6.1 \times 10^4$  cm<sup>2</sup> mol<sup>-1</sup> as the absorption coefficients at 840 and 764 cm<sup>-1</sup> respectively [22,33].

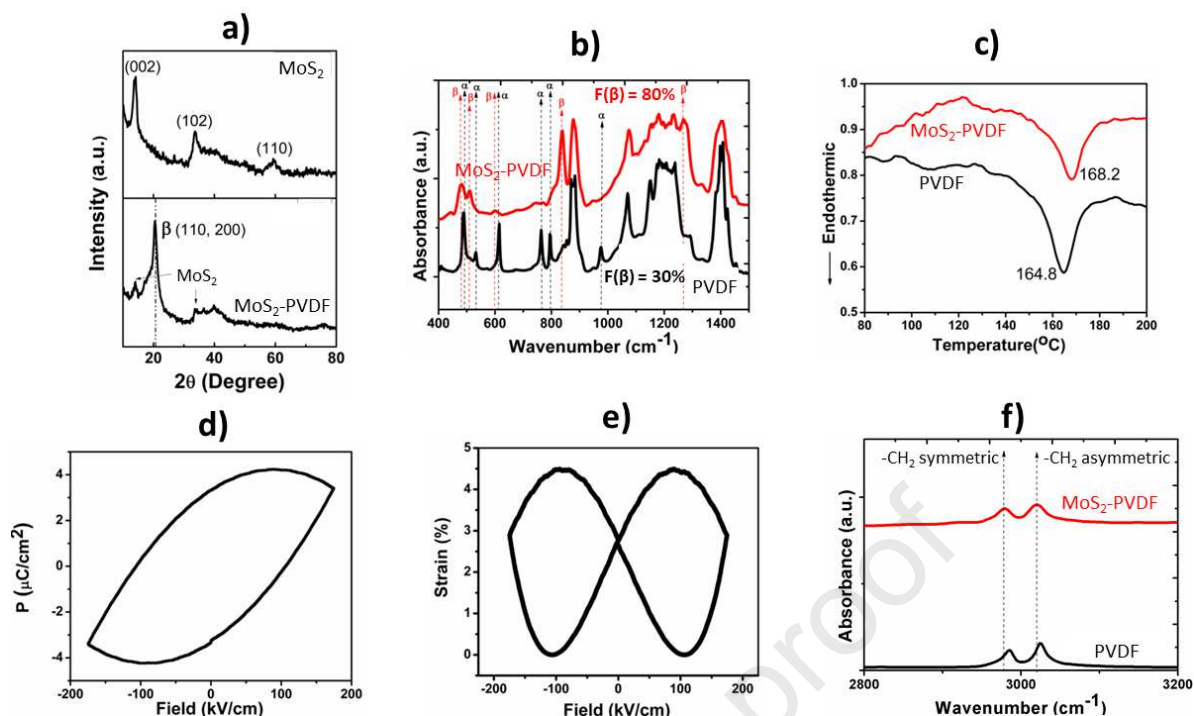


Figure 2: a) X-ray diffraction pattern of MoS<sub>2</sub> and MoS<sub>2</sub>-PVDF film, b) FTIR spectra of the PVDF and the MoS<sub>2</sub>-PVDF films, c) DSC thermographs of the PVDF and the MoS<sub>2</sub>-PVDF films, d) P-E hysteresis loop, e) strain-field butterfly loop for the MoS<sub>2</sub>-PVDF film and f) FTIR spectra showing interaction of MoS<sub>2</sub> with -CH<sub>2</sub> backbone of PVDF.

Using this equation, the  $\beta$  phase crystallization in pure PVDF is found to be 30% whereas for MoS<sub>2</sub>-PVDF it reached 80%. It is noted here that polar solvents like DMF, DMSO, DMAc can also induce  $\beta$  phase to certain extent in native PVDF by interacting with the chain but still require poling to exhibit piezoelectric properties [30]. Since the piezoelectric nature of PVDF is strongly dependent on the amount of electroactive  $\beta$  phase, therefore the addition of MoS<sub>2</sub> nanoparticles clearly enhances its piezoelectric properties.

#### DSC thermograph analysis

The phase crystallization and melting behavior of pure PVDF and MoS<sub>2</sub>-PVDF film was also analyzed by differential scanning calorimetry (DSC) to complement XRD and FTIR measurements. The melting peak at 164.5 °C in the DSC thermograph of pure PVDF film indicates presence of nonpolar  $\alpha$  polymorph [22], whereas for the MoS<sub>2</sub> doped PVDF, the melting peak is shifted to a higher temperature suggesting the nucleation of electroactive  $\beta$  phase in the nanocomposite film (Figure 2c). The degree of crystallinity ( $X_c$ ) of the films have been evaluated by the formula  $X_c = \Delta H_m / \Delta H_{100\%}$ , (where  $\Delta H_m$  is the enthalpy of fusion of the samples and  $\Delta H_{100\%}$  is the enthalpy of fusion of 100% crystallite PVDF(104.6 J/g))

[22, 33]. The enthalpy of fusion and crystallinity both increased upon MoS<sub>2</sub> doping; MoS<sub>2</sub>-PVDF film had  $X_c \approx 53.43\%$  compared to  $X_c \approx 33\%$  for pure PVDF. This change is due to interaction between MoS<sub>2</sub> nanoflowers and the polymer resulting in the formation of  $\beta$ -crystals in the nanocomposite film.

#### *Ferroelectric characterization*

Ferroelectric properties of MoS<sub>2</sub>-PVDF film were determined from the room-temperature polarization-electric field (P-E) hysteresis loop measurements at 50 Hz in the  $\pm 200$  kV/cm range. The area within the loop corresponds to heterogeneous charge density and indicates charge storage capability of the material [22]. As can be seen from Figure 2d, the MoS<sub>2</sub>-PVDF film shows a strong remnant polarization ( $P_r$ ) value of  $3.38 \mu\text{C cm}^{-2}$  compared to pure PVDF ( $0.038 \mu\text{C cm}^{-2}$  at 100 Hz). This high  $P_r$  value can be ascribed to good reversible ferroelectric behaviour and accelerated heterogeneous polarization tendency in the film. It also indicates that the material is inherently polar and piezoelectric in nature [22] since no poling was used in our synthesis process, confirming the self-poling property of these nanocomposite films. Following Katsouras *et al.* [34], the piezoelectric coefficient ( $d_{33}$ ) is calculated using the equation  $d_{33} = -P_r/Y$ , where  $P_r$  and  $Y$  is the remnant polarization and Young's modulus respectively at zero applied electric field (see ESI†). The Young's modulus of the MoS<sub>2</sub>-PVDF film was measured to be  $928 \text{ N/mm}^2$ . Therefore, by using the above equation,  $d_{33}$  of MoS<sub>2</sub>-PVDF comes out to be  $-36.4 \text{ pC/N}$ . This value is higher than observed in poled PVDF [30] ( $24 \text{ pC/N}$ ) showing that the composite film has superior piezoelectric properties without undergoing any poling process. The electrostriction coefficient  $Q_{33}$  was calculated to be  $6.8 \text{ m}^4\text{C}^{-2}$  using the relation  $d_{33} = Q_{33}/2\epsilon\epsilon_0 P_r$ , where  $\epsilon$  is the dielectric constant of the MoS<sub>2</sub>-PVDF film and  $\epsilon_0$  is permittivity of free space ( $8.854 \times 10^{-12} \text{ F m}^{-1}$ ). Based on  $Q_{33}$ , longitudinal strain ( $S_3$ ) under polarization could be calculated by using the equation  $S_3 = Q_{33} P^2$ . Using these strain values, a strain vs field curve was plotted (Figure 2e) which shows a characteristic butterfly loop nature and confirms the reversible polarization and converse piezoelectric behaviour of the nanocomposite film [35].

The above chemical, thermal and electromechanical characterisation establishes the self-poling feature of the MoS<sub>2</sub>-PVDF nanocomposite. In terms of microstructure, we can rationalise the observed self-poling property through either a possible hydrogen bonding or electrostatic interaction between Mo-S dipole in non-centrosymmetric MoS<sub>2</sub> nanoflowers and



characterisation, a more focussed investigation on mechanical and electrical characteristics of this nanocomposite and the role of nanoflower concentration will be required for a deeper understanding of the underlying mechanisms.

#### *FESEM imaging*

The morphology of the piezoelectric films was assessed by FESEM (see Figure 4). MoS<sub>2</sub> particles are spherical in shape with particle size of ~0.8 μm (Figure 4a). A magnified image (Figure 4b) clearly shows that each particle has flower like morphology characteristic of single and few-layers MoS<sub>2</sub> as described by Wu *et al.* [11]. Each nanoflower particle is in turn composed of typical aggregation of nano-petals having thickness of <100 nm (see Figure S1a, ESI†).

MoS<sub>2</sub> impregnated PVDF shows distinct formation of spherulites of diameter ~5-8 μm which confirms β phase crystallization [22] (Figure 4c). The fracture surface of the MoS<sub>2</sub>-PVDF films shows the presence and distribution of MoS<sub>2</sub> nanoflowers in the PVDF matrix (Figure 4d). Most of the MoS<sub>2</sub> is found to be embedded inside the polymer with very little fraction exposed to the environment at porous regions on the surface of the film. Although some local MoS<sub>2</sub> particle aggregation exist but mostly the distribution is uniform in the PVDF matrix where the individual nanoflower particle morphology is maintained (Figure S1b, ESI†).

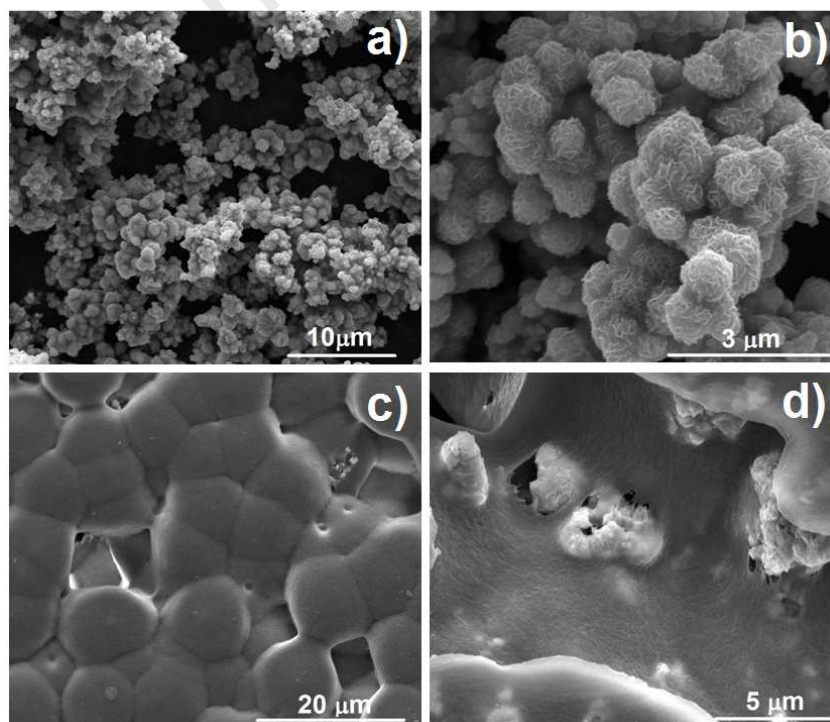


Figure 4: FESEM images of a) hydrothermally synthesized MoS<sub>2</sub> nanoflowers, b) magnified image of the nanoflowers showing abundant single and few layers MoS<sub>2</sub>, c) surface of MoS<sub>2</sub>-PVDF film showing spherulite formation due to  $\beta$  phase crystallization and d) fracture surface of a MoS<sub>2</sub>-PVDF film with embedded MoS<sub>2</sub> nanoflowers.

Elemental mapping (Figure S2, ESI<sup>†</sup>) and EDAX (Figure S3, ESI<sup>†</sup>) was also performed to analyse the distribution of MoS<sub>2</sub> particles in the PVDF matrix. A homogeneous distribution of particles was observed throughout the film which indicates uniform dispersion and interaction with PVDF.

#### *MoS<sub>2</sub>-PVDF nanogenerator (MPNG) performance*

Figure 5 captures the nanogenerator functionality of the MoS<sub>2</sub>-PVDF film (Figure 5a). The device flexibility and layered construction of the package are shown in Figure 5b and Figure 5c, respectively. Both the film and the prototype nanogenerator device (see Figure 5b) are highly flexible and robust, showing excellent energy harvesting capability from mechanical energy. The piezoelectric output of the MPNG device under periodic human finger tapping (~5 Hz) is shown in Figure 5d. An impressive open circuit voltage ( $V_{oc}$ ) of 84V is obtained under a tapping force of 27.5 N and the corresponding short circuit current ( $I_{sc}$ ) reached a value of 3.05  $\mu$ A (Figure 5e).

The variation of the output voltage from MPNG was further evaluated across different load resistances (ranging from 1 to 40 M $\Omega$ ); the instantaneous voltage increased and gradually reached a peak value of 84 V at 30 M $\Omega$  similar to open voltage circuit ( $V_{oc}$ ) (Figure 5g). The corresponding instantaneous current ( $I_L$ ) is calculated by the equation  $I_L = V/R_L$ , where, V is the voltage measured across load resistance  $R_L$ . The effective power density is determined from the equation  $P = (V^2/R_L) 1/v$ , where, v is the effective volume (surface area  $\times$  thickness). The device gave an outstanding peak power density of 47.14 mW cm<sup>-3</sup> at 30 M $\Omega$  load (Figure 5h). To the best of our knowledge, this is the highest power density obtained by finger tapping in MoS<sub>2</sub> nanoparticle doped PVDF which again highlights the synergistic piezoelectric effect in our self-poled nanocomposite film. The observed high power density can be rationalised for two reasons. First, the contributions due to the strain induced piezoelectric potential generated by the self-poled PVDF and the MoS<sub>2</sub> nanoflowers, under vigorous tapping force (~27 N), reinforce each other. Second, we surmise that the vigorous tapping also causes additional strain induced spontaneous polarization and consequent dipole



formation leading to charge separation (electron and hole pairs) and accumulation at the abundant edge sites of piezoelectric MoS<sub>2</sub> nanoflowers and PVDF interface [8, 11, 28]. This should enhance the piezoelectric output. A comparison of the device with other previously reported PVDF based nanogenerators is summarized in ESI† (table S1). In contrast, pure PVDF based nanogenerator only produced 4 V under the same tapping force (see ESI†, Figure S4). The as fabricated device also produced an output of 2V under ultrasonic bath (100 W) condition (see ESI†, Figure S5) which shows that it is highly sensitive over a wide range of frequency.

A possible working mechanism of the device is depicted in Figure 3. Under mechanical stress, the polarization produced (by separation of charges) in the piezoelectric film (see Figure 3) can be harnessed in terms of electric power by using electrodes on either side of the film which drives the electrons through the external circuit. When the stress is released, the electrons flow in the opposite direction and a negative potential is reached [8-11, 28, 35]. To demonstrate the application potential of the as fabricated MPNG, it was connected to a 1 $\mu$ F capacitor through a bridge rectifier. As shown in Figure 5f, the capacitor is charged very swiftly to 2.5 V within 20 s under finger tapping (see Table S2, ESI† for comparison). Further, the device was able to power up 25 commercial LEDs when connected in series through a full wave bridge rectifier (Figure 5i and video S1, ESI†) showing that they can be promising candidates for developing portable self-powered electronic and medical devices.

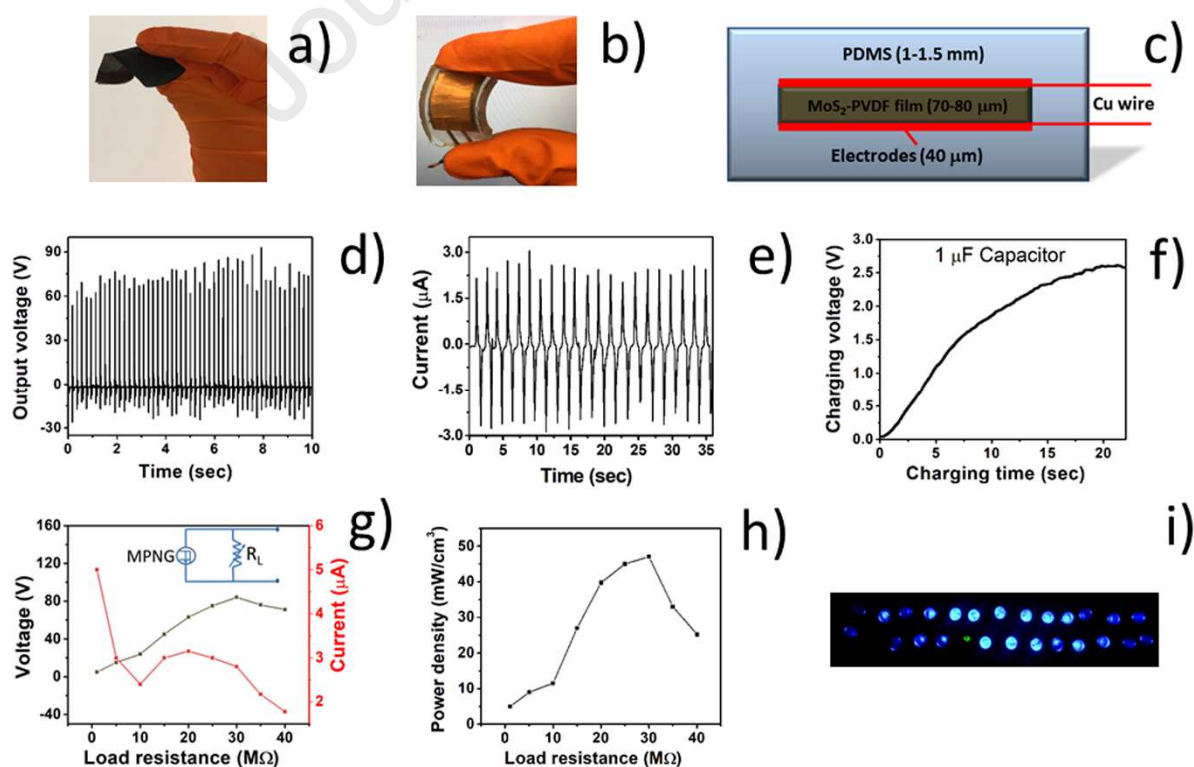


Figure 5: a) Flexible MoS<sub>2</sub>-PVDF film, b) nanogenerator prototype (i.e. the MPNG), c) schematic showing MPNG fabrication design. Performance of MPNG under continuous human finger tapping, d) open circuit voltage ( $V_{oc}$ ), e) short circuit current ( $I_{sc}$ ), f) capacitor charging, g) variation of voltage and current across with different load resistances (1 M $\Omega$  to 40 M $\Omega$ ), inset shows the corresponding circuit diagram, h) effective power density variation with different load resistances (1 M $\Omega$  to 40 M $\Omega$ ) and i) powering up commercial LED bulbs.

### *Piezocatalytic dye degradation*

Piezocatalytic dye degradation was monitored using UV-Visible spectroscopy. As observed from Figure 6, the dyes showed rapid degradation within 20 minutes of ultrasonication with the nanocomposite MoS<sub>2</sub>-PVDF film in dark condition. The degradation can be visually observed (see Figure S6, ESI<sup>†</sup>) from the change in dye colour after 25 minutes of ultrasonication thereby clearly demonstrating their piezocatalytic property. In contrast, pure PVDF film failed to any appreciable degradation of dyes even after prolonged sonication (50 mins) (Figure S7, ESI<sup>†</sup>).

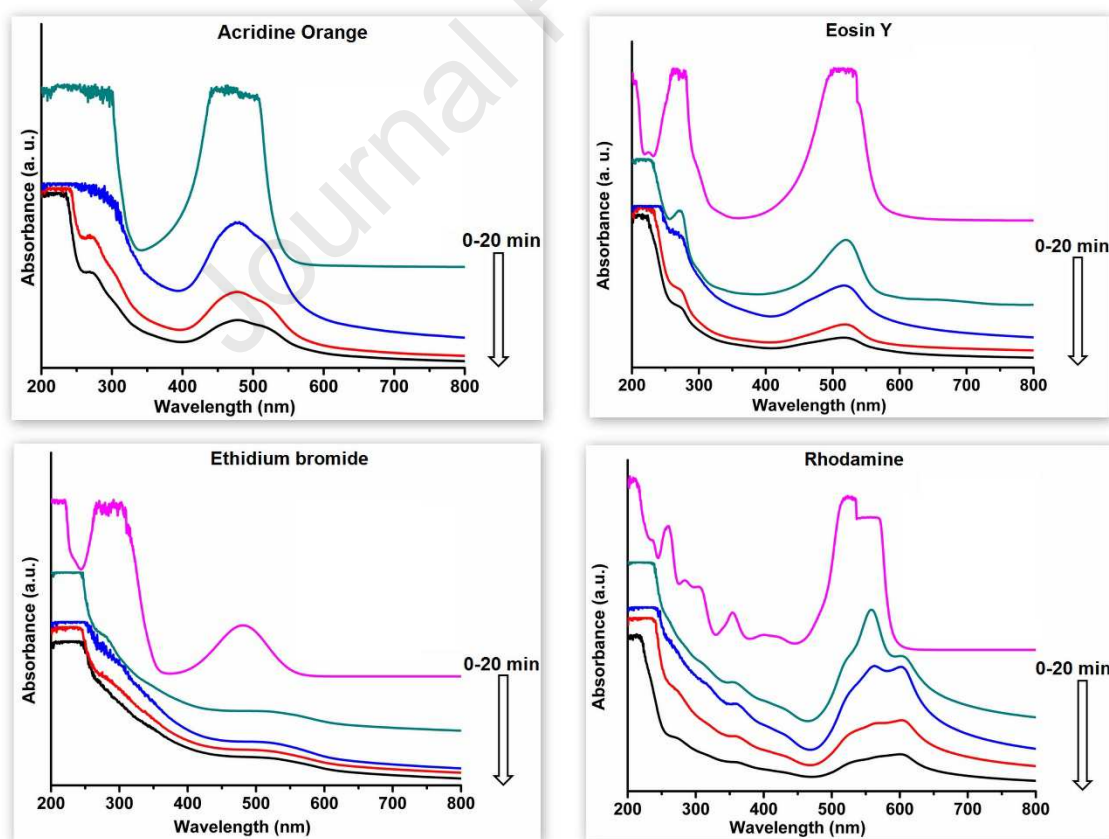


Figure 6: UV-Visible spectra of dyes undergoing piezocatalytic degradation under ultrasonic vibration in dark- Acridine orange (top left), Eosin Y (top right), Ethidium bromide (bottom left) and Rhodamine B (bottom right).

The percent degradation over time is presented in Figure 7a, where the MoS<sub>2</sub>-PVDF film shows excellent catalytic activity in dark with >90% degradation achieved for each dye. However, with undoped PVDF film, the amount of dyes remained unchanged even after prolonged ultrasonication which indicates that the piezoelectric effect in MoS<sub>2</sub>-PVDF film is playing a major role in the catalytic process. The degradation reaction followed pseudo first order kinetics as indicated from the rate of degradation curve (Figure 7b). The highest rate constant was achieved for Ethidium bromide (ET) (0.32 min<sup>-1</sup>) followed by Eosin Y (0.26 min<sup>-1</sup>), Rhodamine B (0.21 min<sup>-1</sup>) and Acridine Orange (0.127 min<sup>-1</sup>), respectively. To date, degradation of these dyes has been mainly limited to using photocatalytic nanoparticles (ZnO, TiO<sub>2</sub>, SnO<sub>2</sub>, Fenton's reagent, Au and Ag etc) under light irradiation [22-25, 37-41]. In contrast, in the present case this is achieved by MoS<sub>2</sub>-PVDF film through a fast-piezo driven catalytic process which harnesses vibrational energy to degrade dyes under dark conditions, which are more suited to industrial effluents flowing through pipelines. Although MoS<sub>2</sub> nanoflowers – in powder form – has been reported to degrade Rhodamine B [8, 10, 11] but this is the first time where a nanocomposite is shown to piezocatalytically degrade potentially carcinogenic dyes like Ethidium bromide, Eosin Y and Acridine Orange.

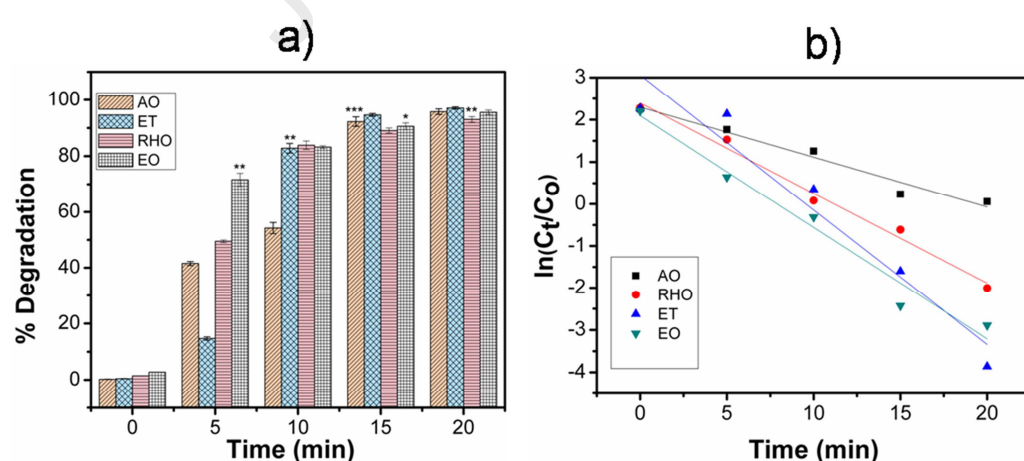


Figure 7: a) Variation in dye degradation by MoS<sub>2</sub>-PVDF film and b) the rate of degradation over time. C<sub>0</sub>- initial concentration (10 ppm), C<sub>t</sub>- concentration at time t. Values are ±

standard error of the mean of five experiments done in triplicate (one way ANOVA). \* $p > 0.05$ , \* $p > 0.005$  and \* $p > 0.0005$ .

Based on this observation, a piezocatalytic mechanism of dye degradation is proposed as presented in Figure 8 below. As already mentioned, incorporation of MoS<sub>2</sub> nanoflowers converts an otherwise unpoled piezoelectric PVDF to a self-poled and highly piezoelectric nanocomposite. Since MoS<sub>2</sub> is already piezocatalytic, therefore its inclusion in the PVDF matrix results in boosting the piezoelectric as well as piezocatalytic property of the overall nanocomposite. Thus, when the piezoactive MoS<sub>2</sub>-PVDF film is subjected to ultrasonic vibrations in an aqueous solution containing dye, MoS<sub>2</sub> nanoflowers are mechanically agitated to generate electron-hole pairs by spontaneous polarization of MoS<sub>2</sub> nanoflowers. This polarization is further enhanced by the interaction of MoS<sub>2</sub> with PVDF where piezoelectric  $\beta$  phase is induced. These electron and hole pairs then migrate (in opposite direction) and accumulate to the film surface aided by the dispersed MoS<sub>2</sub> particles in PVDF. Continuous rapid vibration by ultrasound generates and accumulates enough electrons and holes at the film surface to split water form ROS like  $\cdot\text{OH}$ ,  $\cdot\text{O}^-$  etc. Hence, the organic dye molecules are rapidly degraded by the produced ROS similar to a photocatalytic process [8, 10, 11] (Figure 8a). However, it may be mentioned here that surface of the film (SEM image in Figure 4d) contains scattered porous regions where MoS<sub>2</sub> is partially exposed to the dye solution and thus will contribute to dye degradation as well.

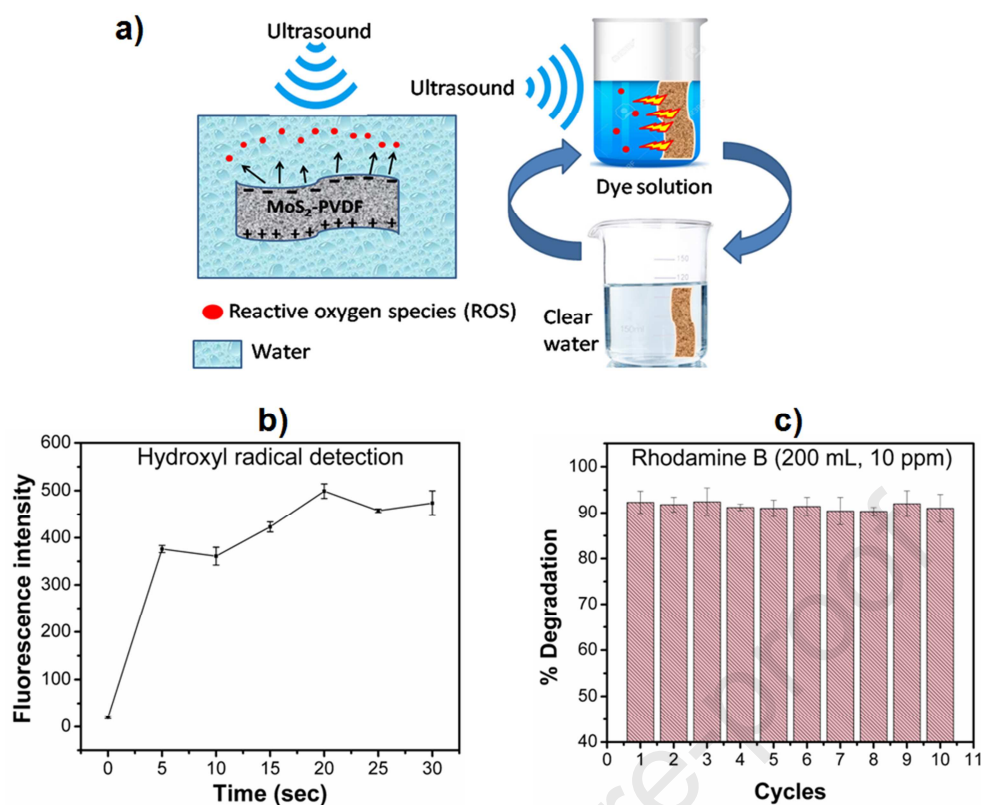


Figure 8: a) Mechanism of piezocatalysis of the MoS<sub>2</sub>-PVDF film, b) hydroxyl radical evolution under ultrasonic bath vibration and c) re-usability test of MoS<sub>2</sub>-PVDF film showing stable degradation of Rhodamine B for 10 cycles.

Lin *et al.* [31], reported piezocatalytic activity, where they used MoS<sub>2</sub> nanoflower-PDMS to degrade Rhodamine B in running water. However, the piezocatalytic activity solely came from exposed MoS<sub>2</sub> on the PDMS surface and showed deterioration in activity with time with time due to spillage when the composite is subjected to friction with water. In case of our MoS<sub>2</sub>-PVDF nanocomposite however, as explained by XRD, FTIR and SEM, since MoS<sub>2</sub> actively induces  $\beta$  phase by interacting with the PVDF chain, therefore it leads to a more robust attachment where we believe that MoS<sub>2</sub> will be held more strongly in PVDF compared to PDMS at this loading concentration (i.e, 10 wt% MoS<sub>2</sub>). A time lapse photo of the film immersed in the Rhodamine B dye solution and subjected to ultrasonic vibration is presented in Figure S8 (ESI<sup>†</sup>) showing gradual decolorization of the water without any apparent degradation of the film over a period of 25 min. However, when the film was loaded with 20% (w/w) MoS<sub>2</sub>, the water turned greyish due to spillage of the excess MoS<sub>2</sub> particles, nevertheless showed much faster degradation of dyes as already reported by Wu *et al.* [8,11].

The mechanical stimulus driven generation of  $\cdot\text{OH}$  radical in the dye solution is confirmed by trapping it with terephthalic acid at regular intervals under ultrasound agitation. Terephthalic acid forms a fluorescent hydroxyterephthalic acid upon reaction with  $\cdot\text{OH}$  radical, which offers qualitative means to detect the radical formation with high sensitivity [42]. From Figure 8b, it can be observed that  $\cdot\text{OH}$  radical is being gradually generated with time after ultrasound exposure and reaching a stable value around 20 minutes which coincides with the catalytic degradation time. One of the main advantages of using  $\text{MoS}_2$ -PVDF films in water purification would be their reusability since the nanocomposite is inherently piezocatalytic and mechanically robust. In order to assess this feature, the piezocatalysis experiment was repeated using the same film with fresh solution of Rhodamine B (200 mL, 10 ppm). The result presented in Figure 8c shows stable catalytic performance over 10 cycles with >90% efficiency using 200 mL of dye solution under dark conditions. However, since the volume is large the degradation time was over 40 mins. This also confirms the robustness of our PVDF based nanocomposite film in contrast to the work of Lin *et al.* [31], where the catalytic activity decreased with progressive cycle (67% at 4<sup>th</sup> cycle) due to release of  $\text{MoS}_2$  particles from PDMS surface. FESEM of the film surface post experiment (Figure S9, ESI<sup>†</sup>) shows that structural integrity is maintained even after repeated use. Thus, the developed piezocatalytic film provides safe and reliable production of on-demand ROS which may be applied to degrade ecotoxic organic and inorganic pollutants from water reservoirs, drainage and sewer systems where photocatalytic application is not feasible or is difficult to implement.

## Conclusion

This work summarizes the synthesis of a highly robust, efficient and self-poled piezoelectric nanocomposite and applies them to two key areas namely water remediation and energy harvesting. The nanocomposite showed strong piezocatalytic activity as demonstrated by a rapid and efficient degradation (>90%) of some potentially carcinogenic dyes under ultrasound vibrations within a short time of 20 min. Such catalytic reaction is found to be initiated by production of reactive oxygen species in aqueous solution as a result of strong piezoelectric effect by the nanocomposite film under dark condition as opposed to photocatalysis which requires light. The origin of piezoelectricity in the nanocomposite film was studied in detail by using different analytical and electrical measurements and shows that  $\text{MoS}_2$  nanoflowers plays a vital role in inducing the  $\beta$  crystals in PVDF which results in spontaneous orientation of dipoles leading to self-poled piezoelectricity in the nanocomposite

film. Also, the overall functionality of the nanocomposite is enhanced due to entrapment of inherently piezoelectric and piezocatalytic MoS<sub>2</sub> nanoflowers in the polymer matrix. The films are robust and reusable and showed promise of purifying large volume of dye contaminated water (200 mL) over 10 cycles using only vibrational energy. In addition, the nanocomposite has been successfully exploited as an efficient energy harvesting device (nanogenerator) which can be activated by mechanical vibrations from common human and natural activities. The nanogenerator produced a maximum output voltage of 84 V and a power density of 47.14 mW cm<sup>-3</sup> under human finger tapping which powered up 25 LED lights instantaneously. Overall, the development of such advanced and versatile piezoelectric nanocomposite materials opens up a novel, energy efficient way to develop novel water remediation technologies and smart self-powered electronic devices.

## References

- [1] R. Loos, R. Carvalho, D. C. António, S. Comero, *et al.*, EU-wide monitoring survey on emerging polar organic contaminants in wastewater treatment plant effluents. *Water Res.* 47 (2013) 6475-6487.
- [2] C. C. Wang, J. R. Li, X. L. Lv, Y. Q. Zhang, G. Guo, Photocatalytic organic pollutants degradation in metal–organic frameworks, *Energy Environ Sci.*, 7 (2014) 2831-2867.
- [3] J. Rivera-Utrilla, M. Sánchez-Polo, M. A. Ferro-García, G. Pradoz-Joya, R. Ocampo-Pérez, Pharmaceuticals as emerging contaminants and their removal from water. A review, *Chemosphere*, 93 (2013) 1268-1287.
- [4] M. M. Khin, S. S. Nair, V. J. Babu, R. Murugan, S. Ramakrishna, A review on nanomaterials for environmental remediation, *Energy Environ Sci*, 5(2012) 8075-8109.
- [5] H. Lachheb, E. Puzenat, A. Houas, M. Ksibi, E. Elaloui, C. Guillard and J. M. Herrmann. Photocatalytic degradation of various types of dyes (Alizarin S, Crocein Orange G, Methyl Red, Congo Red, Methylene Blue) in water by UV-irradiated titania, *Appl Catal B*, 39 (2002) 75–90.
- [6] J. Blackbeard, J. Lloyd, M. Magyar, J. Mieog, K. G. Linden, Y. Lester, Demonstrating organic contaminant removal in an ozone-based water reuse process at full scale *Environ. Sci.: Water Res. Technol.* 2 (2016)213-223.

- [7] M. A. Mallick, A. Ghaffar, S. A. Mallick, Water purification by electrical discharges, *Plasma Sources Sci. Technol.* 10 (2001) 82–91.
- [8] J. M. Wu, Y. G. Sun, W. E. Chang, J.T. Lee, Piezoelectricity induced water splitting and formation of hydroxyl radical from active edge sites of MoS<sub>2</sub> nanoflowers, *Nano Energy*, 46 (2018) 372-382.
- [9] N. A. Shepelin, A. M. Glushenkov, V. C. Lussini, P. J. Fox, G. W. Dicoski, J. G. Shapter, A. V. Ellis, New developments in composites, copolymer technologies and processing techniques for flexible fluoropolymer piezoelectric generators for efficient energy harvesting, *Energy Environ Sci.* 12 (2019) 1143-1176.
- [10] M. B. Starr and X. Wang, Fundamental analysis of piezocatalysis process on the surfaces of strained piezoelectric Materials, *Sci. Rep.* 3 (2013) 2160-2168.
- [11] J. M. Wu, W. E. Chang, W. T. Chang and C. Chang, Piezo-catalytic effect on the enhancement of the ultra-high degradation activity in the dark by single- and few-layers MoS<sub>2</sub> nanoflowers. *Adv. Mater.* 28 (2016) 3718–3725.
- [12] H. Van Acker, T. Coenye, The role of reactive oxygen species in antibiotic-mediated killing of bacteria, *Trends Microbiol.* 25(6) (2017) 456-466.
- [13] T. G. Dong, S. Dong, C. Catalano, R. Moore, X Liang and J. J. Mekalanos, Generation of reactive oxygen species by lethal attacks from competing microbes, *Proc. Natl. Acad. Sci.* 112 (2015) 2181-2186.
- [14] G. Tan, S. Wang, Y. Zhu, L. Zhou, *et al.*, Surface-selective preferential production of reactive oxygen species on piezoelectric ceramics for bacterial killing. *ACS Appl. Mater. Interfaces*, 37(8) (2016) 24306-24309.
- [15] S. Lan, J. Feng, Y. Xiong, S. Tian, S. Liu, L. Kong, Performance and mechanism of piezo-catalytic degradation of 4-Chlorophenol: finding of effective piezo-dechlorination, *Environ. Sci. Technol.* 51(2017) 6560-6569.
- [16] H. Lin, Z. Wu, Y. Jia, W. Li, R. K. Zheng, H. Luo, Piezoelectrically induced mechano-catalytic effect for degradation of dye wastewater through vibrating Pb(Zr<sub>0.52</sub>Ti<sub>0.48</sub>)O<sub>3</sub> fibers *Appl. Phys. Lett.* 104(2014) 1629071-1629074.
- [17] Y. Yang, H. Zhang, S. Lee, D. Kim, W. Hwang, Z. L. Wang, Hybrid energy cell for degradation of methyl orange by self-powered electrocatalytic oxidation, *Nano Lett.* 13(2013) 803–818.



- [18] C. F. Tan, W. L. Ong, G. W. Ho, Self-biased hybrid piezoelectric-photoelectrochemical cell with photocatalytic functionalities. *ACS Nano* 9(2015) 97661–7670.
- [19] D. Hong, W. Zang, X. Guo, Y. Fu, H. He, J. Sun, L. Xing, B Liu, X. Xue, High piezo-photocatalytic efficiency of CuS/ZnO nanowires using both solar and mechanical energy for degrading organic dye, *ACS Appl. Mater. Interfaces* 8 (2016) 21302–21314.
- [20] X. Xue, W. Zang, P. Deng, Q. Wang, L. Xing, Y. Zhang, Z. Wang, Piezo-potential enhanced photocatalytic degradation of organic dye using ZnO nanowires *Nano Energy*, 13(2015) 414–422.
- [21] M. K. Lo, S. Y. Lee, K. S. Chang, Study of ZnSnO<sub>3</sub>-nanowire piezophotocatalyst Using Two-Step Hydrothermal Synthesis, *J. Phys.Chem. C* 119(2015) 5218–5224.
- [22] N. A. Hoque, P. Thakur, S. Roy, A. Kool, B. Bagchi, P. Biswas, M. Saikh, F. Khatun, S. Das, P. P. Ray, Er<sup>3+</sup>/Fe<sup>3+</sup> Stimulated electroactive, visible light emitting, and high dielectric flexible PVDF film based piezoelectric nanogenerators: A simple and superior self-powered energy harvester with remarkable power density. *ACS Appl. Mater. Interfaces* 9(27) (2017)23048–23059.
- [23] C. S. Lu, C. C. Chen, L. K. Huang, P. A. Tsai, H. F. Lai, Photocatalytic degradation of Acridine Orange over NaBiO<sub>3</sub> driven by visible light irradiation catalysts, 3(2013), 501-516.
- [24] H. Zheng, Y. Pan, X. Xiang, Oxidation of acidic dye Eosin Y by the solar photo-Fenton processes. *J. Hazard. Mater.* 141(2007) 457-464.
- [25] C. Adán, A. Martínez-Arias, M. Fernández-García, A. Bahamonde, Photocatalytic degradation of ethidium bromide over titania in aqueous solutions, *Appl. Catal B- Environ.* 76(2007) 395–402.
- [26] Y. S. Safitri, I. W. A. Indrawan, S. Winarsih, Rhodamine B induces oxidative stress and cervical epithelial cell proliferation in the uterus, *Toxicol Rep.* 2(2015) 1434-1436.
- [27] K. Cai, X. Han, Y. Zhao, R. Zong, F. Zeng, D. Guo, A green route to a low cost anisotropic MoS<sub>2</sub>/Poly(Vinylidene Fluoride) nanocomposite with ultrahigh electroactive phase and improved electrical and mechanical properties, *ACS Sustain Chem. Eng.* 6(2018) 5043–5052.
- [28] K. Maity, B. Mahanty, T. K. Sinha, S. Garain, A. Biswas, S. K. Ghosh, S. Manna, S. K. Ray, D. Mandal, Two-dimensional piezoelectric MoS<sub>2</sub>-modulated nanogenerator and nanosensor made of poly(vinylidene fluoride) nanofiber webs for self-powered electronics and robotics, *Energy Technol.* 5(2017) 234-243.
- [29] P. Sahatiya, S. Kannan, S. Badhulika, Few layer MoS<sub>2</sub> and in situ poled PVDF nanofibers on low cost paper substrate as high performance piezo-triboelectric hybrid

nanogenerator: Energy harvesting from handwriting and human touch, *Appl Mater Today*, 13(2018), 91-99.

[30] P. Martins, A.C. Lopes, S. L. Mendez, Electroactive phases of poly(vinylidene fluoride): Determination, processing and applications, *Prog. Polym. Sci.* 39(2014) 683-706.

[31] J. H. Lin, Y. H. Tsao, M. H. Wu, T. M. Chou, Z. H. Lin, J. M. Wu, Single- and few-layers MoS<sub>2</sub> nanocomposite as piezo-catalyst in dark and self-powered active sensor, *Nano Energy* 31(2017) 575-581.

[32] J. Ge, K. Deng, W. Cai, J. Yu, X. Liu, J. Zhou, Effect of structure-directing agents on facile hydrothermal preparation of hierarchical  $\gamma$ -Al<sub>2</sub>O<sub>3</sub> and their adsorption performance toward Cr(VI) and CO<sub>2</sub> *J. Colloid Interface Sci.* 401(2013) 34-39.

[33] P. Thakur, A. Kool, B. Bagchi, S. Das, P. Nandy, In situ synthesis of Ni(OH)<sub>2</sub> nanobelt modified electroactive poly(vinylidene fluoride) thin films: remarkable improvement in dielectric properties, *Phys. Chem. Chem. Phys.* 17(2015) 1368-1378.

[34] I. Katsouras, K. Asadi, M. Li, T. B. van Driel, K. S. Kjær, D. Zhao, T. Lenz, Y. Gu, P. W. M. Blom, D. Damjanovic, M. M. Nielsen, D. M. de Leeuw The negative piezoelectric effect of the ferroelectric polymer poly(vinylidene fluoride), *Nat. Mater.* 15 (2016) 78-84.

[35] N. A. Hoque, P. Thakur, P. Biswas, M. Saikh, S. Roy, B. Bagchi, S. Das, P. P. Ray, Biowaste crab shell-extracted chitin nanofiber-based superior piezoelectric nanogenerator, *J. Mater. Chem. A* 6(2018)13848–13858.

[36] M. Remškar, I. Iskra, J. Jelenc, S. Davorškapin, B. Vîsíc, A. Varlec, A. Křzan, A novel structure of polyvinylidene fluoride (PVDF) stabilized by MoS<sub>2</sub> nanotubes, *Soft Matter* 9(2013) 8647-8653.

[37] R. Ullah, J. Dutta, Photocatalytic degradation of organic dyes with manganese-doped ZnO nanoparticles *J. Hazard Mater.* 156(2008) 194–200.

[38] C. Adân, A. Bahamonde, A. Martínez-Arias, M. Fernández-García, L. A. Pérez Estrada, S. Malato, Solar light assisted photodegradation of ethidium bromide over titania-based catalysts, *Catal. Today* 129(2007) 79-85.

[39] K. Vinodgopal, P. V. Kamat, Enhanced rates of photocatalytic degradation of an Azo dye using SnO<sub>2</sub>/TiO<sub>2</sub> coupled semiconductor thin films, *Environ. Sci. Technol.* 29(1995) 841-845.

[40] S. Mondal, M. E. De Anda Reyes, U. Pal, Plasmon induced enhanced photocatalytic activity of gold loaded hydroxyapatite nanoparticles for methylene blue degradation under visible light, *RSC Adv.* 7(2017) 8633-8645.

[41] X. Liu, M. Liang, M. Liu, R. Su, M. Wang, W. Qi, Z. He, Highly efficient catalysis of azo dyes using recyclable silver nanoparticles immobilized on tannic acid-grafted eggshell membrane, *Nanoscale Res. Lett.* 11 2016 440-449.

[42] M. Sahni, B. R. Locke, Quantification of hydroxyl radicals produced in aqueous phase pulsed electrical discharge reactors, *Ind. Eng. Chem. Res.* 45(2006) 5819-5825.

### **Conflicts of interest**

There are no conflicts of interest to declare.

### **Acknowledgement**

This work is partially supported by the Wellcome/EPSRC Centre for Interventional and Surgical Sciences (WEISS) (203145Z/16/Z) and the NICEDROPS project supported by the European Research Council (ERC) under the European Union's Horizon 2020 research and innovation programme under grant agreement no. 714712.



**Biswajoy Bagchi** received his BSc. in Chemistry (2005) from Calcutta University and MSc. in Biotechnology (2007) and PhD in Material Sciences from Jadavpur University (2013) in India. Currently, he is a postdoctoral research fellow at Wellcome-EPSCRC Centre for Interventional and Surgical Sciences, University College London (UCL) and jointly works with Mechanical Engineering department (UCL). His research focuses on developing therapeutic antimicrobial nanocomposites and scaffold materials and piezoelectric/triboelectric nanocomposites for biomedical sensors and energy harvesting applications.



**Nur Amin Hoque** is a postdoctoral research fellow at Ocean College, Zhejiang University, PR China. He has completed his Undergraduate and Postgraduate in Physics from Jadavpur University, India. In 2018 he earned his Ph.D. His research interests lie in development of piezoelectric and high dielectric polymeric materials for designing effective piezoelectric nanogenerator, triboelectric nanogenerator, wearable electronics, piezo-catalyst, Li/ Na ion cell, solar cell, ferroelectric perovskite materials development for photovoltaic application and self-charged photo-power-cell.



**Norbert Janowicz** obtained MChem from Manchester Metropolitan University (MMU) in 2017 with research project focusing on Microwave Dielectric Spectroscopy study of TiO<sub>2</sub> pigment suspensions. Worked on interdisciplinary projects with Microbiology and Material Chemistry for applications of zeolites in anticorrosive coatings and delaying food degradation. Currently pursuing PhD at UCL focusing on fluorine-free and transparent superhydrophobic coatings utilising various methods such as AACVD, Spin coating and Spray coating of polymer-particle nanocomposites.



**Sukhen Das** is a Professor and Head of the department, Department of Physics, Jadavpur University (India). He has been working as a Scientist-B and Scientist-C in CGCRI, India in his initial years before joining Jadavpur University. He has guided several doctoral and post-doctoral fellows. Currently his research deals with advanced nano and quantum dot materials for development of energy harvesting device, medical applications, antimicrobial bio-ceramics and water purification for health and environment. Professor Das published more than 250 international papers and 5 patents. Author awarded Best Researcher for the year of 2014-2015 by University Grants Commission (Govt. of India).



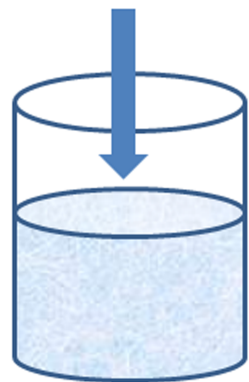
**Manish K Tiwari** is a Royal Society Wolfson Fellow and Professor of Nanoengineering in UCL Mechanical Engineering. He is also ERC Starting Grant awardee, a platform-lead in UCL's Wellcome/EPSCRC Centre for Interventional and Surgical Sciences and a joint-lead in the Manufacturing Future Lab in UCL East. He received PhD from the University of Illinois at Chicago (UIC) and was a Group leader in ETH Zurich, before joining UCL as a Lecturer in late 2013 to establish Nanoengineered Systems Laboratory. With his team, collaborators and industry

partners, Professor Tiwari works on small-scale thermofluidics and manufacturing for energy and healthcare applications.

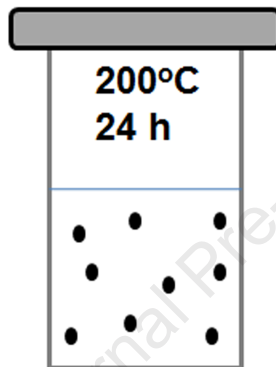
Journal Pre-proof

**Pluronic F127**  
**Ammonium heptamolybdate**  
**Thiourea**

**Hydrothermal treatment**



30 min  
Stirring

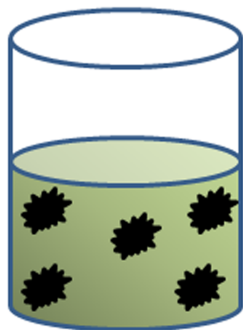


Centrifuge  
10,000 rpm, 10 min

**MoS<sub>2</sub> nanoflowers**



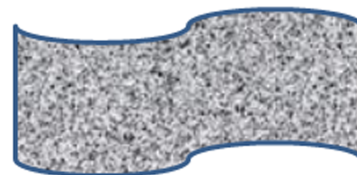
**PVDF (in DMSO) + MoS<sub>2</sub>**

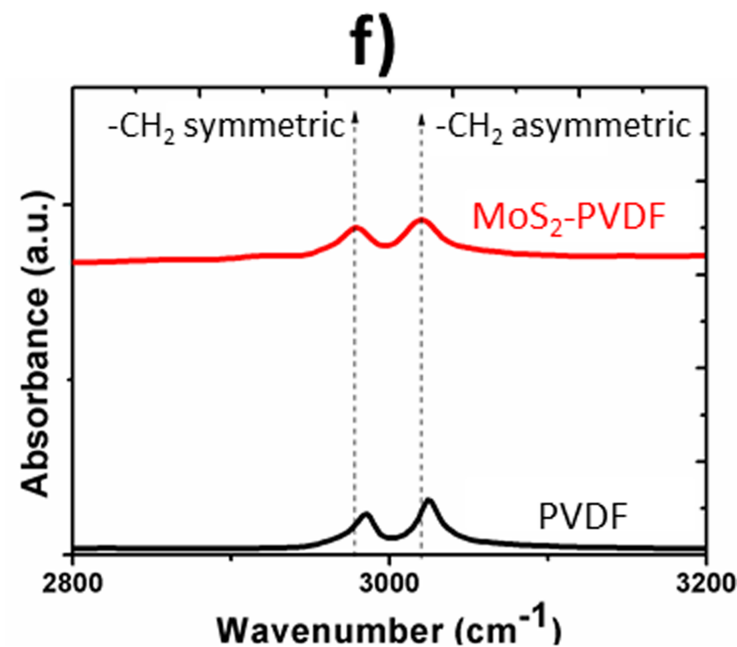
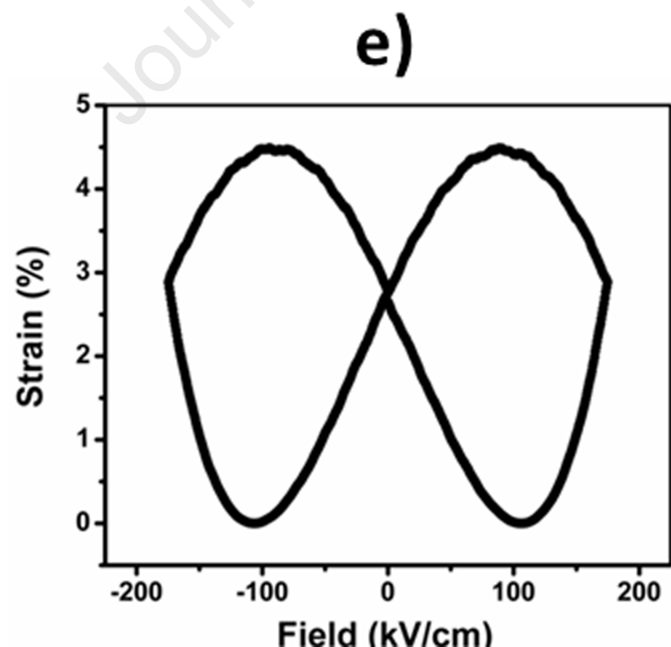
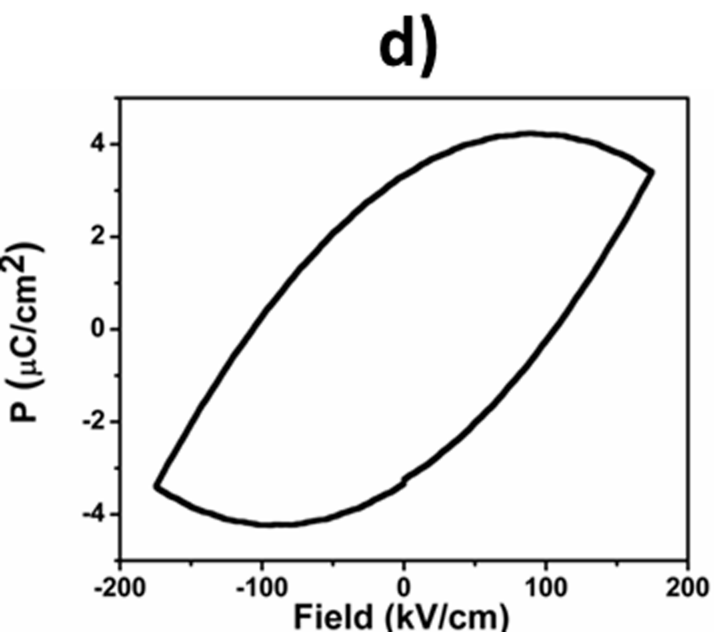
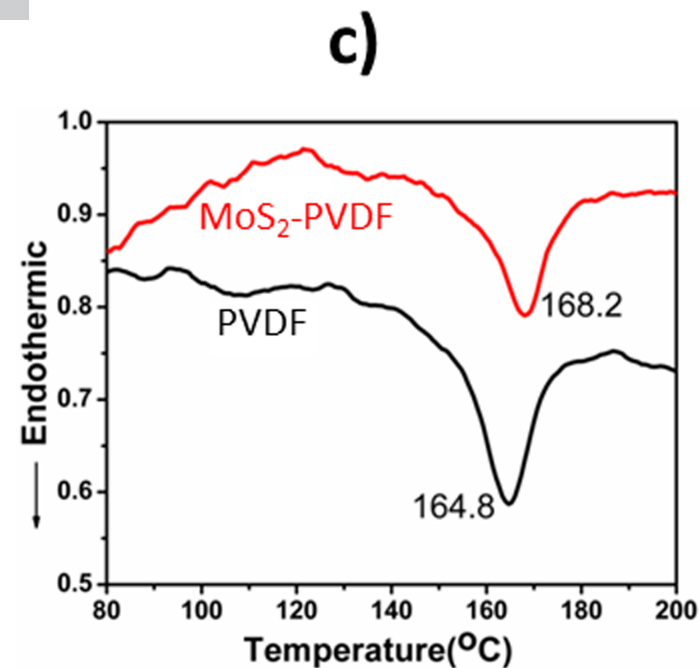
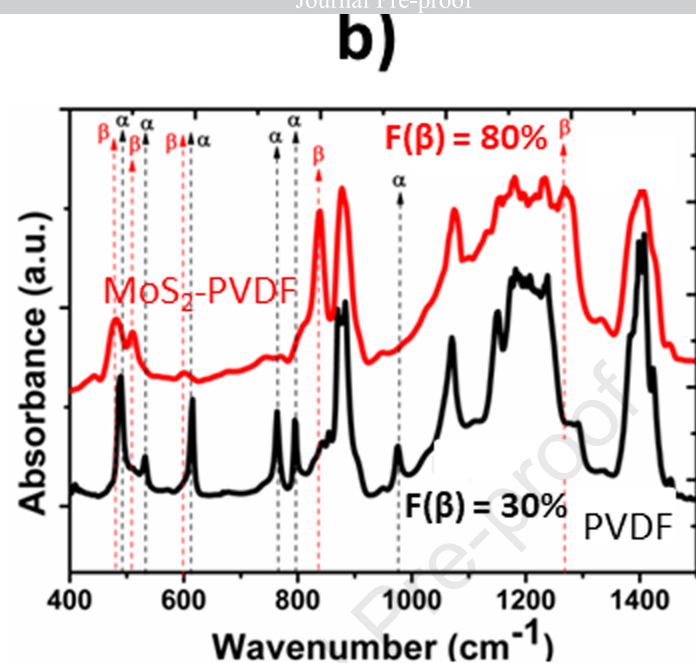
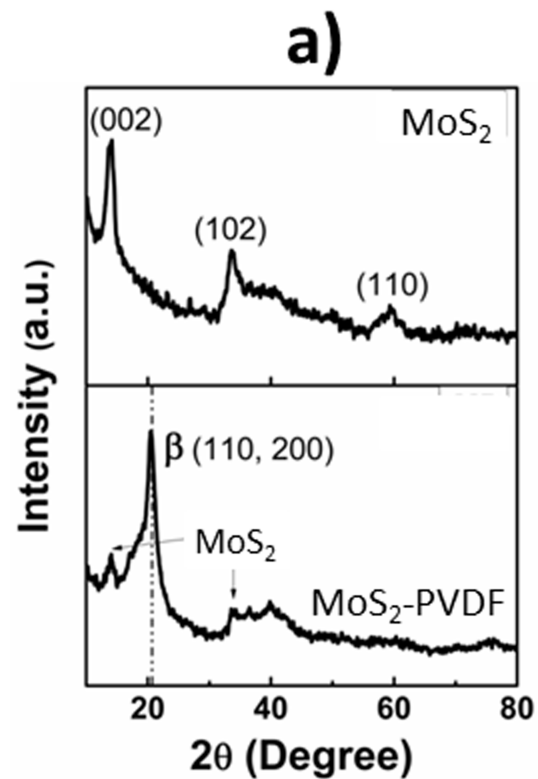


**I. Mixing and solution casting**

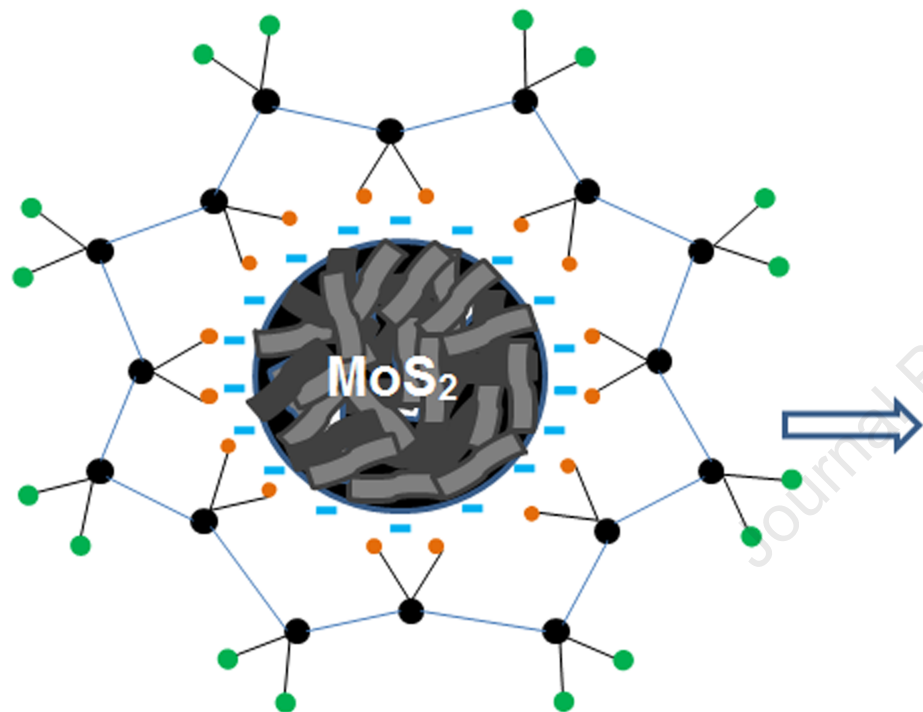
**II. Drying at 80°C**

**MoS<sub>2</sub>-PVDF film**

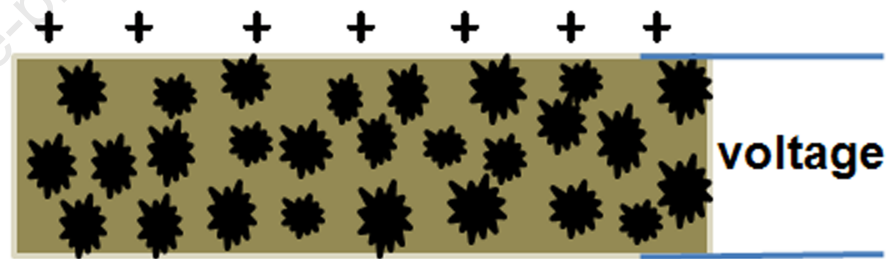





# $\beta$ phase crystallization in PVDF





Mechanical stress/vibrations





MoS<sub>2</sub>-PVDF film

 MoS<sub>2</sub> nanoflower

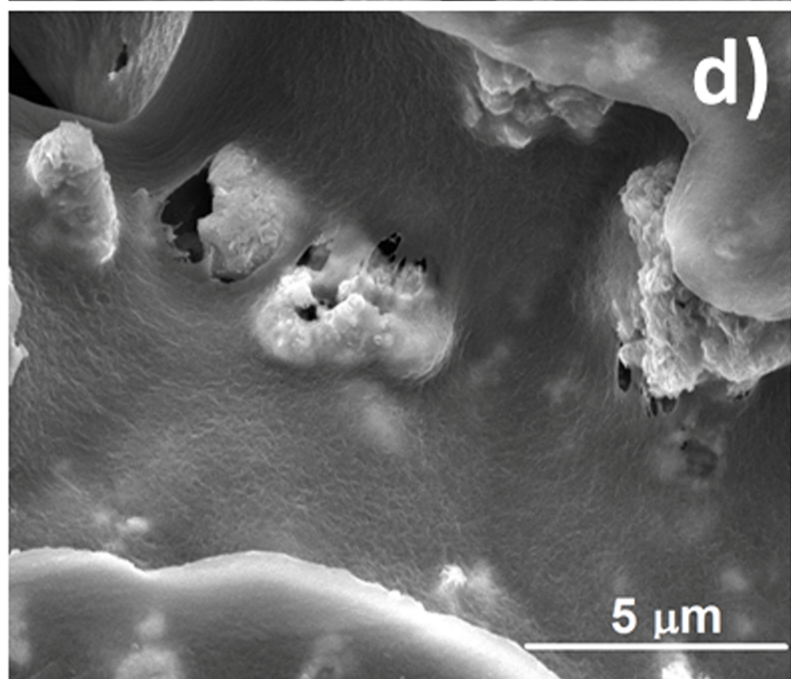
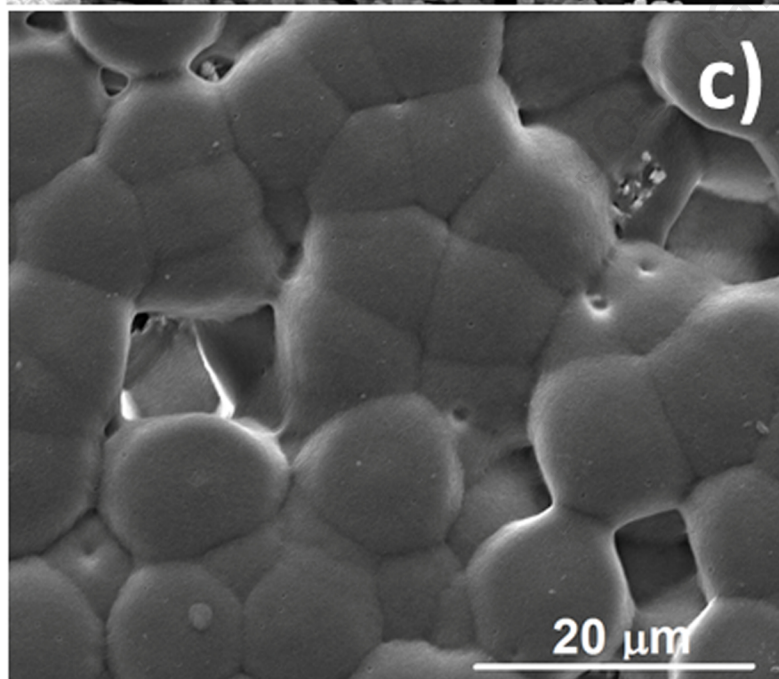
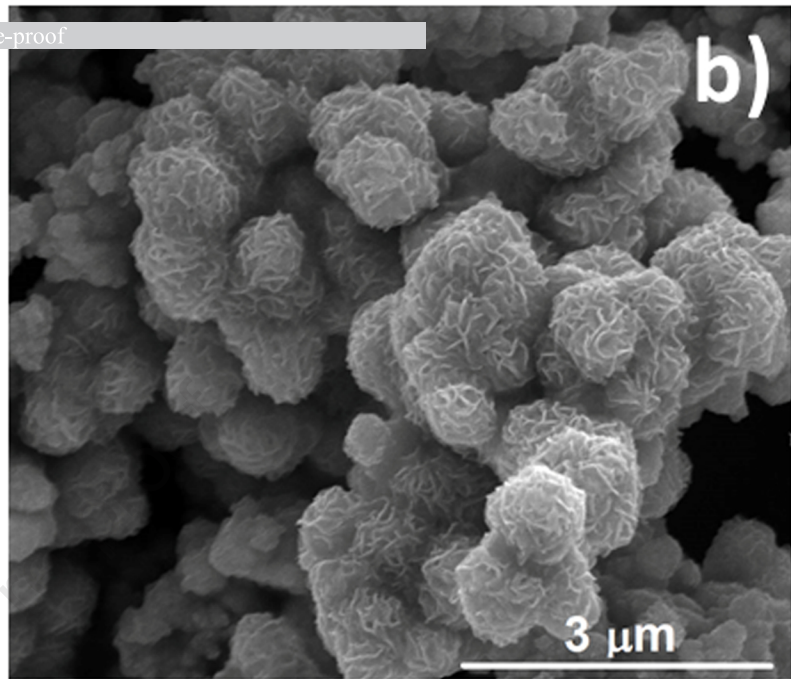
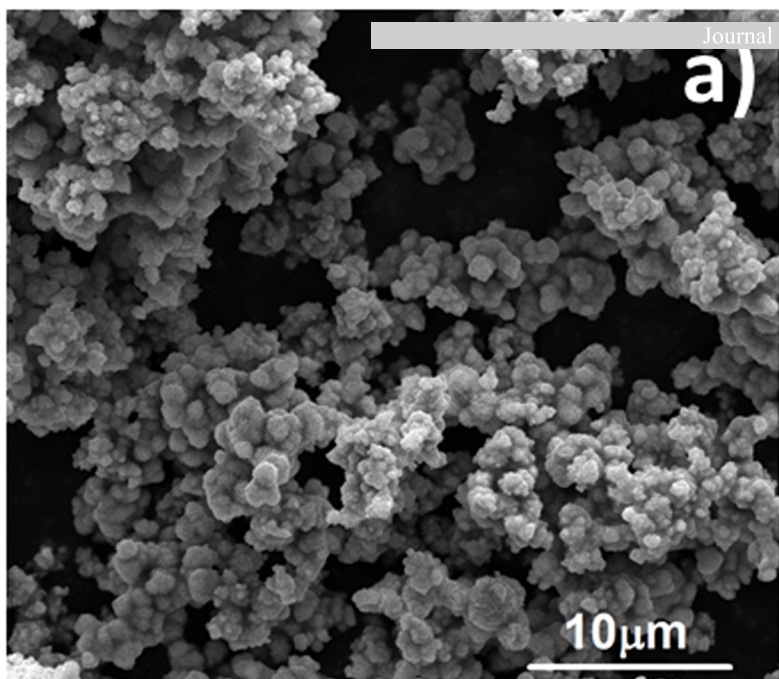
 Negative charge (MoS<sub>2</sub>)

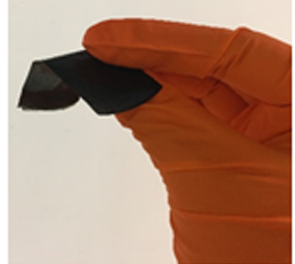
 Fluorine

 Carbon

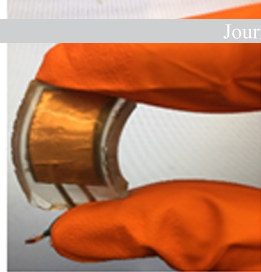
 Hydrogen



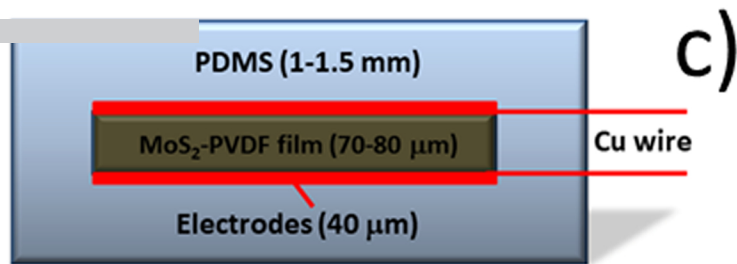




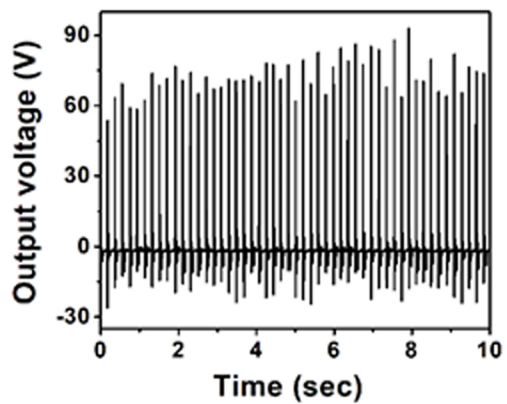
a)



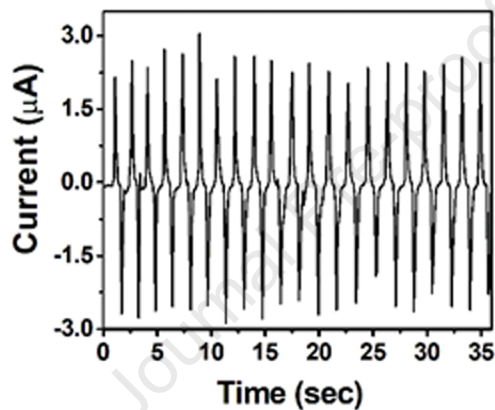
b)



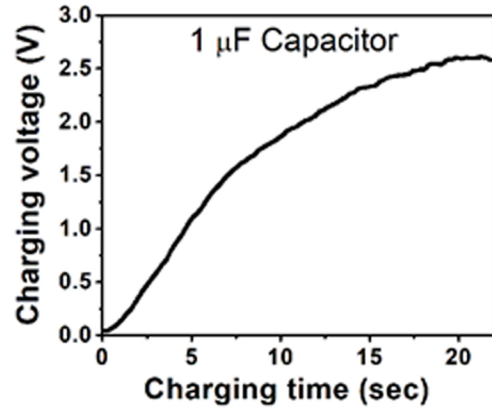
c)



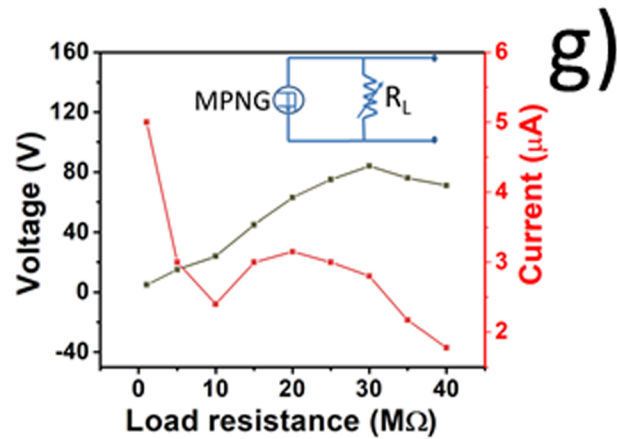
d)



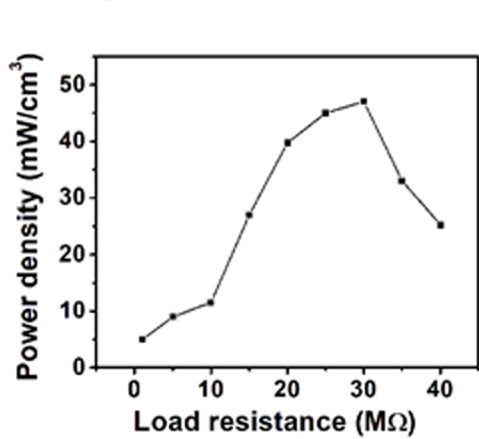
e)



f)



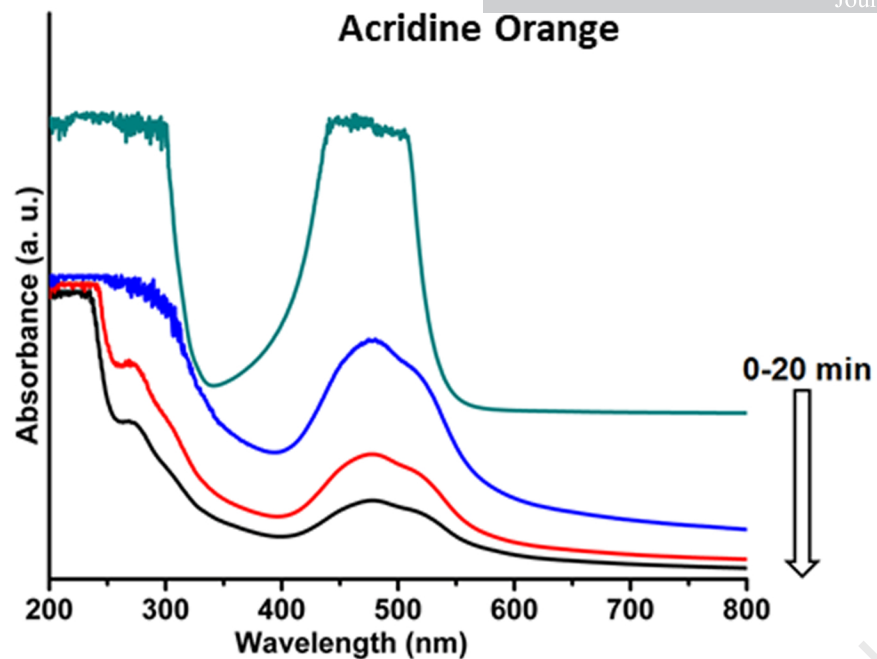
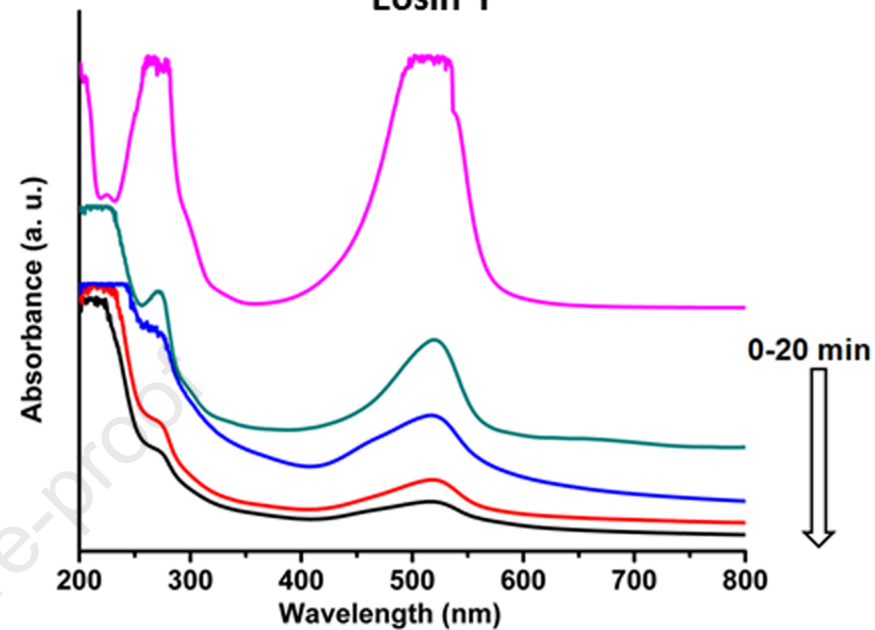
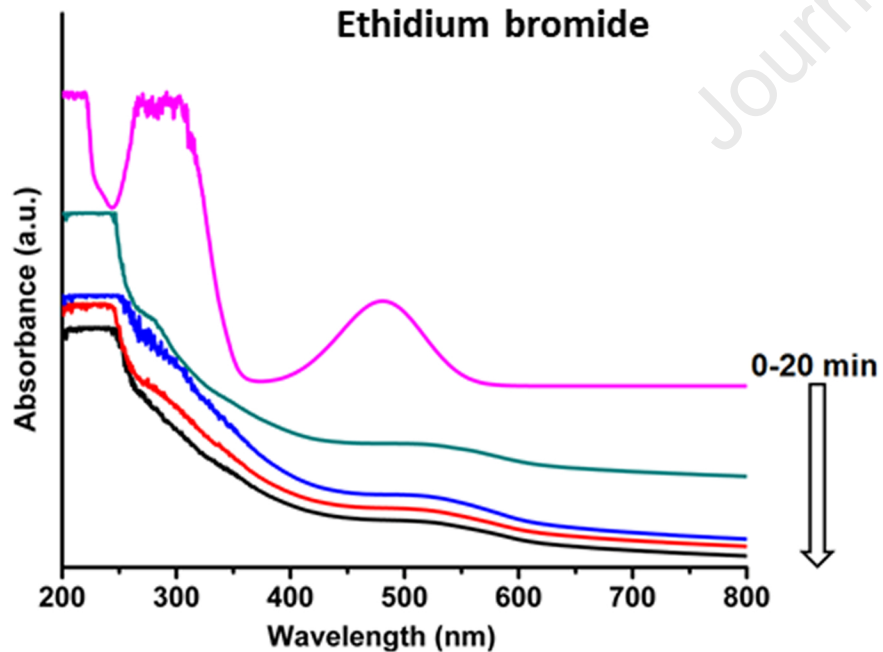
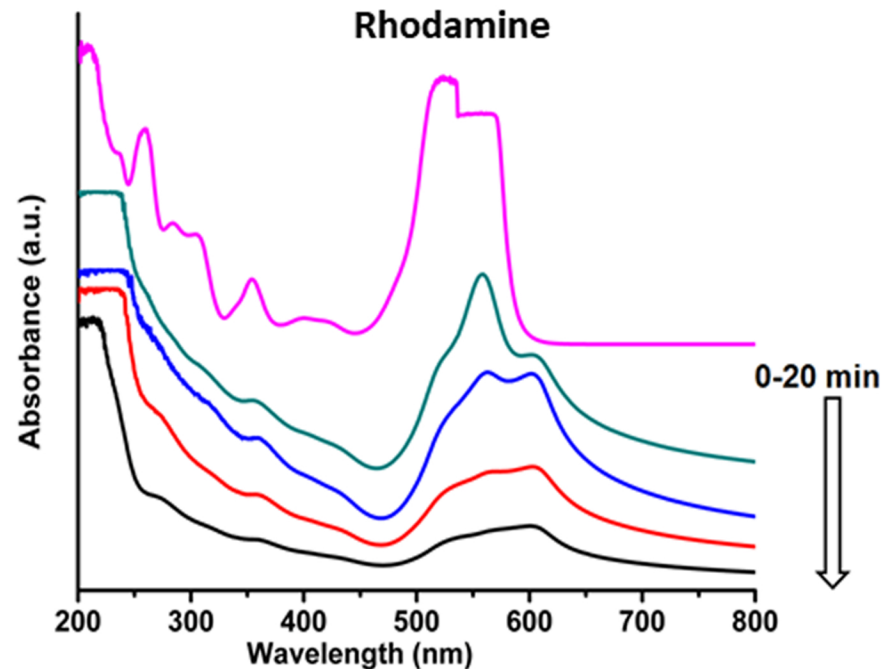
gg)



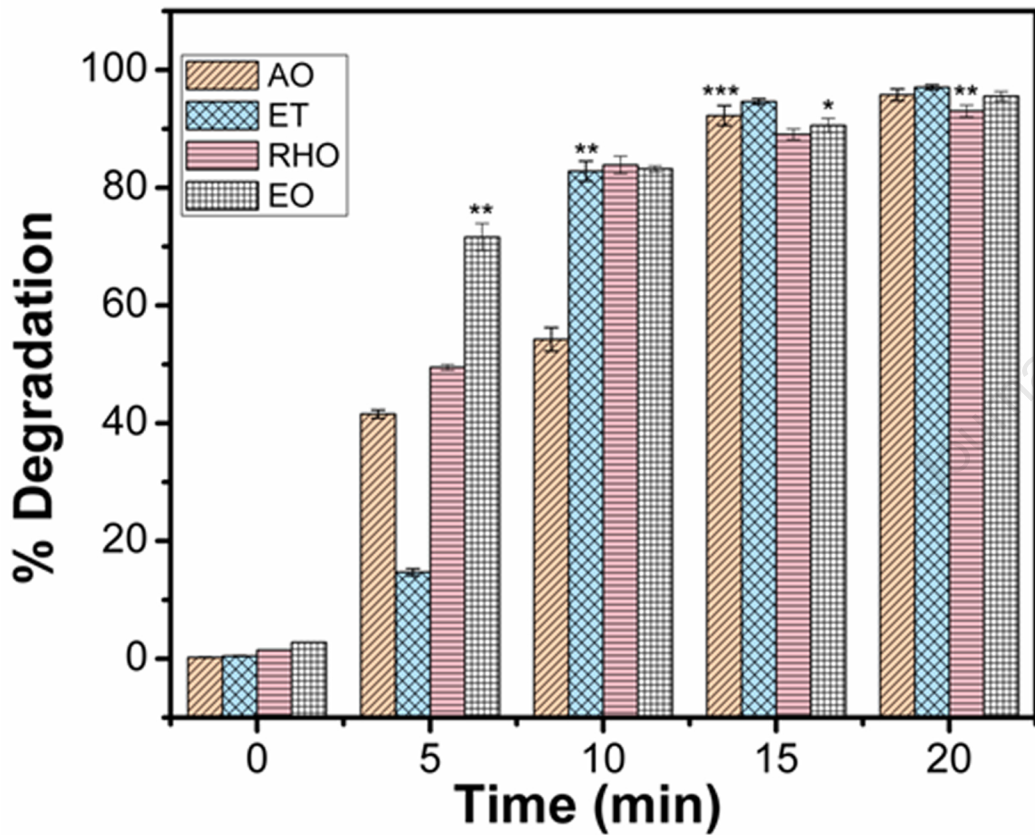
h)



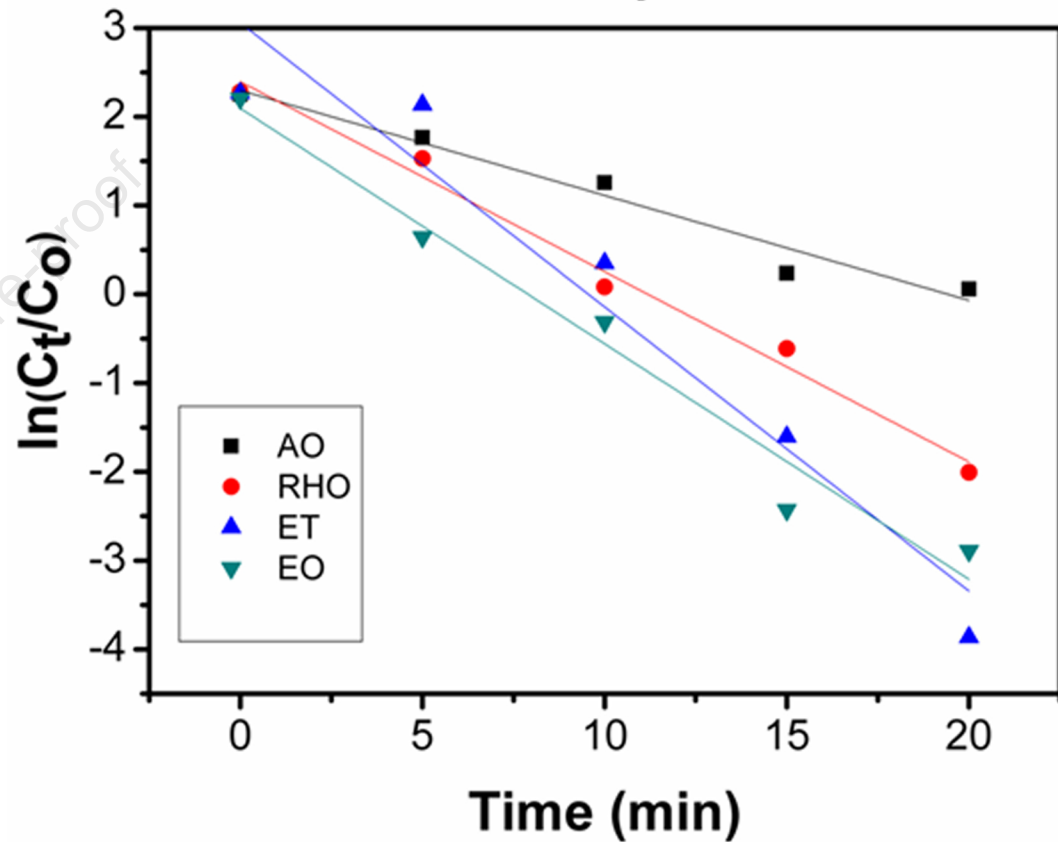
i)

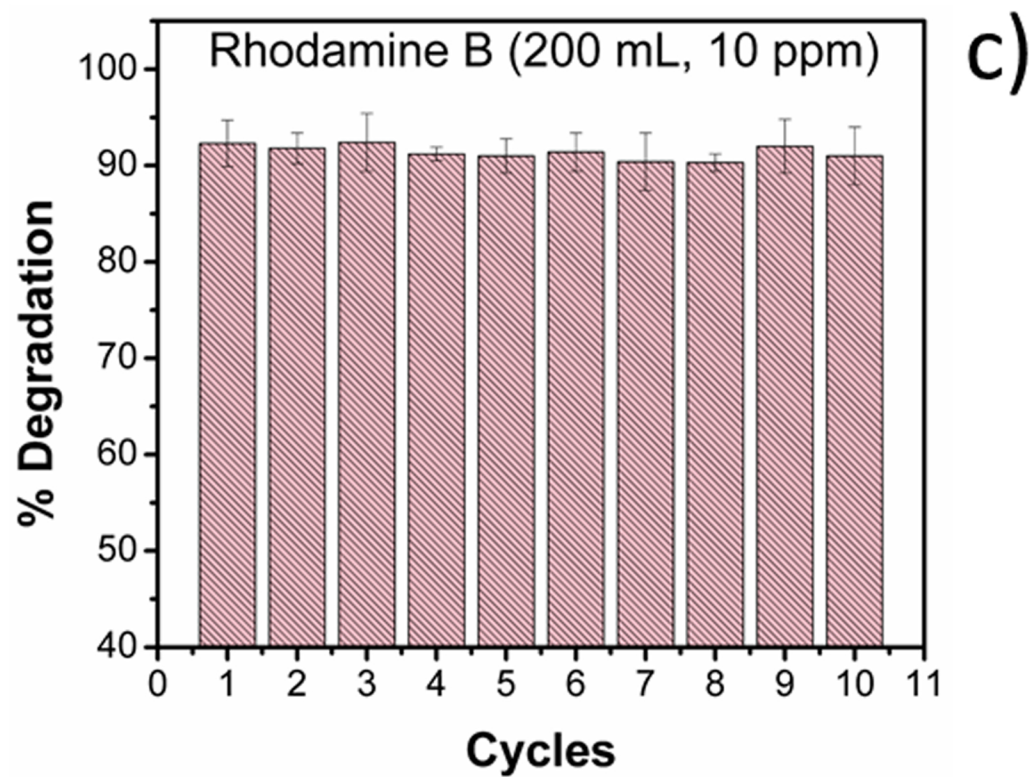
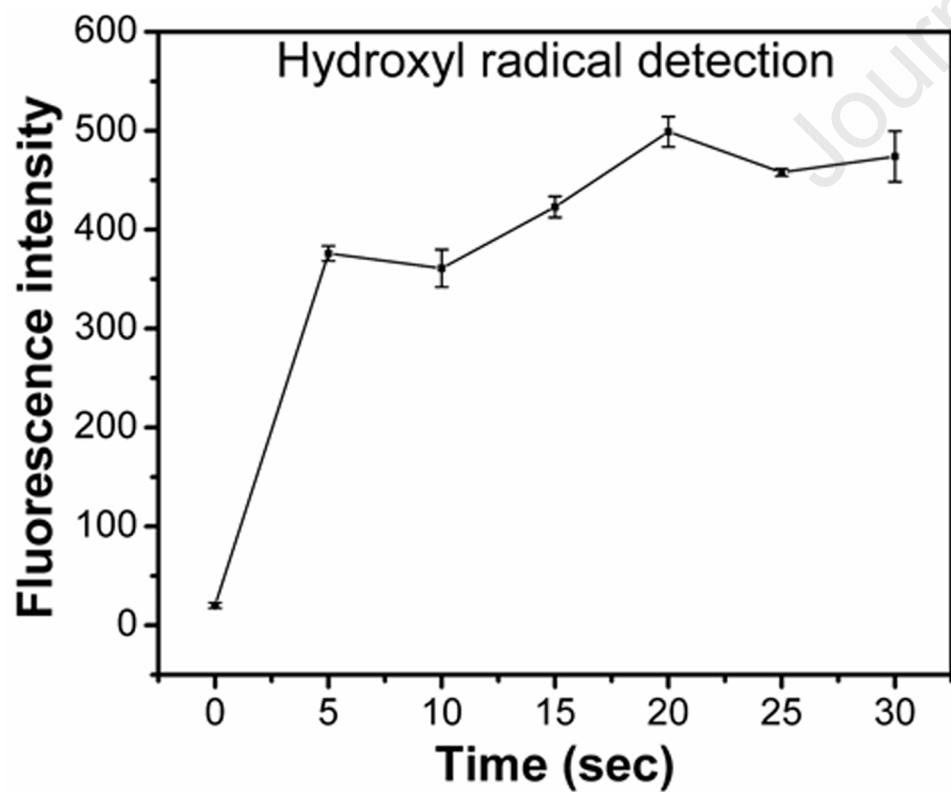
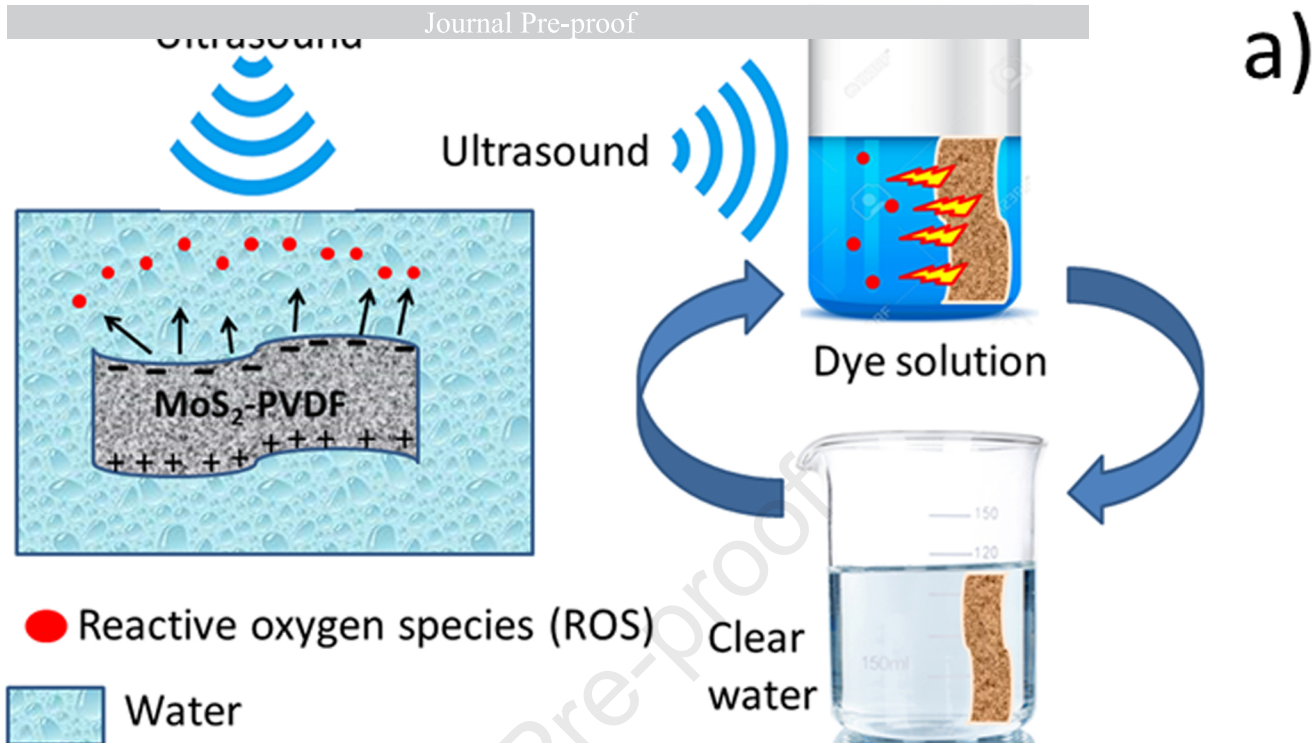
**Acridine Orange****Eosin Y****Ethidium bromide****Rhodamine**

a)



b)





## Electronic Supplementary Information

### Re-usable, self-poled piezoelectric/piezocatalytic films with exceptional energy harvesting and water remediation capability

Biswajoy Bagchi<sup>1,2</sup>, Nur Amin Hoque<sup>3</sup>, Norbert Janowicz<sup>2</sup>, Sukhen Das<sup>3</sup> Manish K. Tiwari<sup>\*1,2</sup>

<sup>1</sup>Wellcome/EPSRC Centre for Interventional and Surgical Sciences, UCL, London, W1W 7TS, UK

<sup>2</sup>Nanoengineered Systems Laboratory, Mechanical Engineering, UCL, London, WC1E 7JE, UK

<sup>3</sup>Jadavpur University, Department of Physics, Kolkata, 700032, India

\*Corresponding author

E-mail: m.tiwari@ucl.ac.uk, Contact: +442031081056

### SEM of MoS<sub>2</sub> nanoflower and MoS<sub>2</sub>-PVDF nanocomposite film

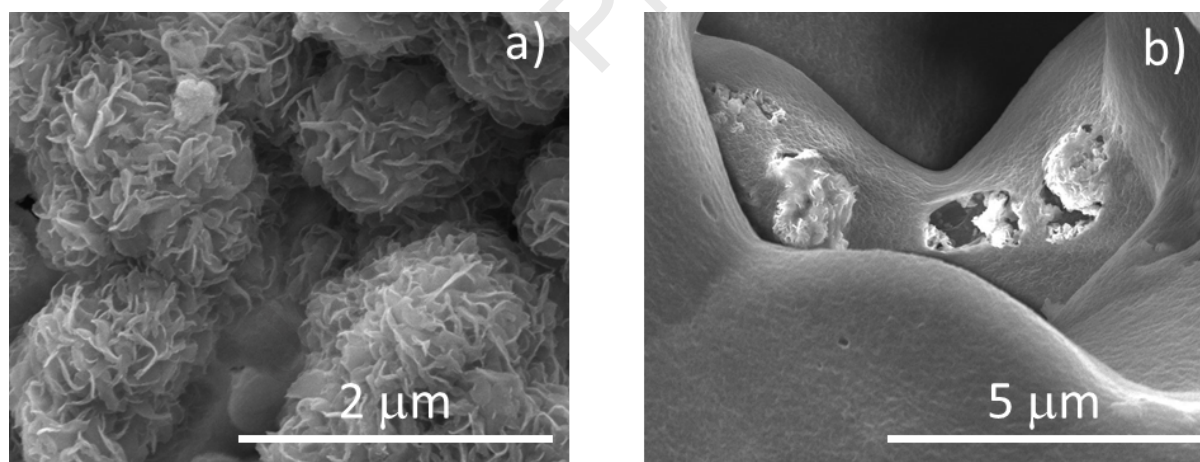


Figure S1: SEM micrographs showing a) microstructure of MoS<sub>2</sub> nanoflower particles which are composed single or few layers of nanopetals and b) distribution of nanoflower particle as observed on the surface of the MoS<sub>2</sub>-PVDF film.

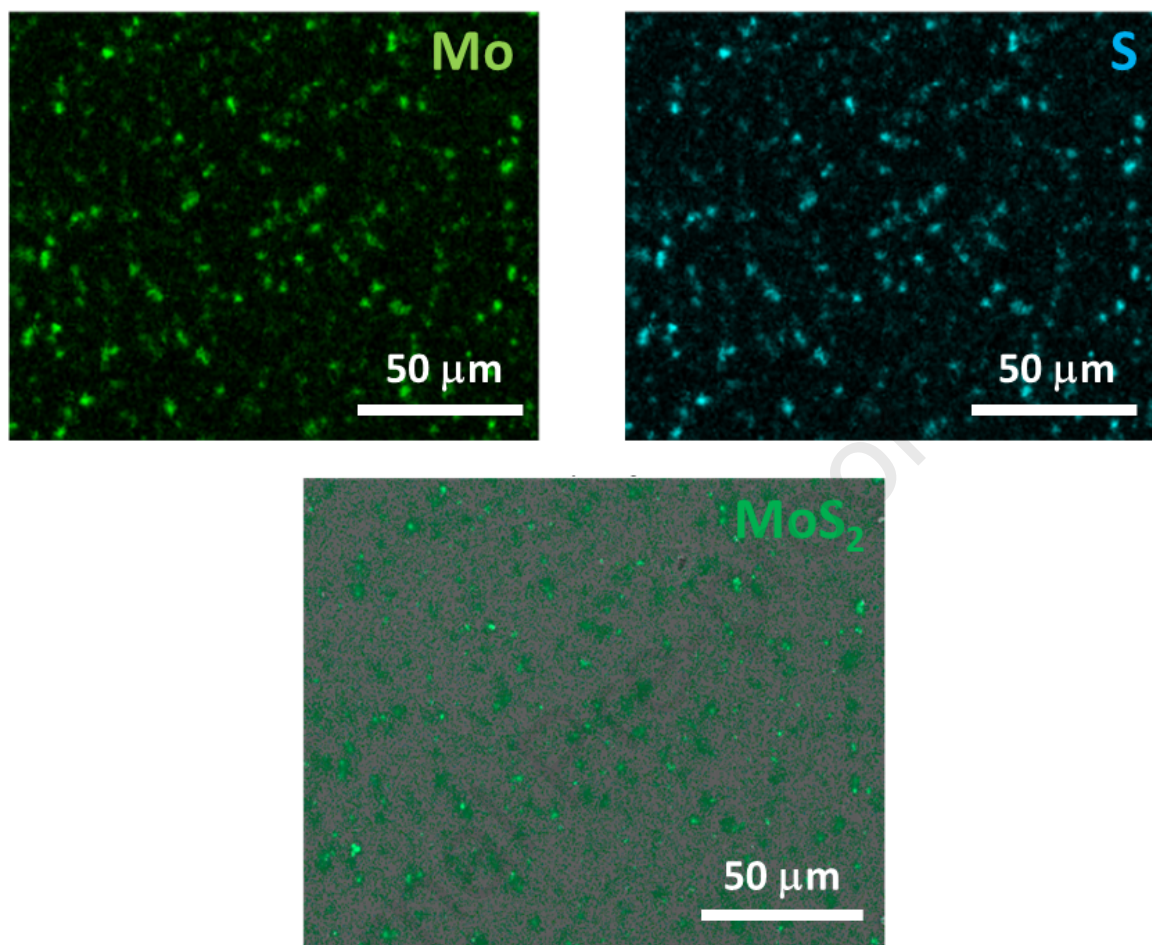
Elemental mapping and EDAX spectra of MoS<sub>2</sub>-PVDF

Figure S2: Elemental mapping of the surface of MoS<sub>2</sub>-PVDF piezoelectric film showing distribution of molybdenum (Mo, top left image), Sulphur (S, top right image) and overlapped image (below) of MoS<sub>2</sub> as a whole.

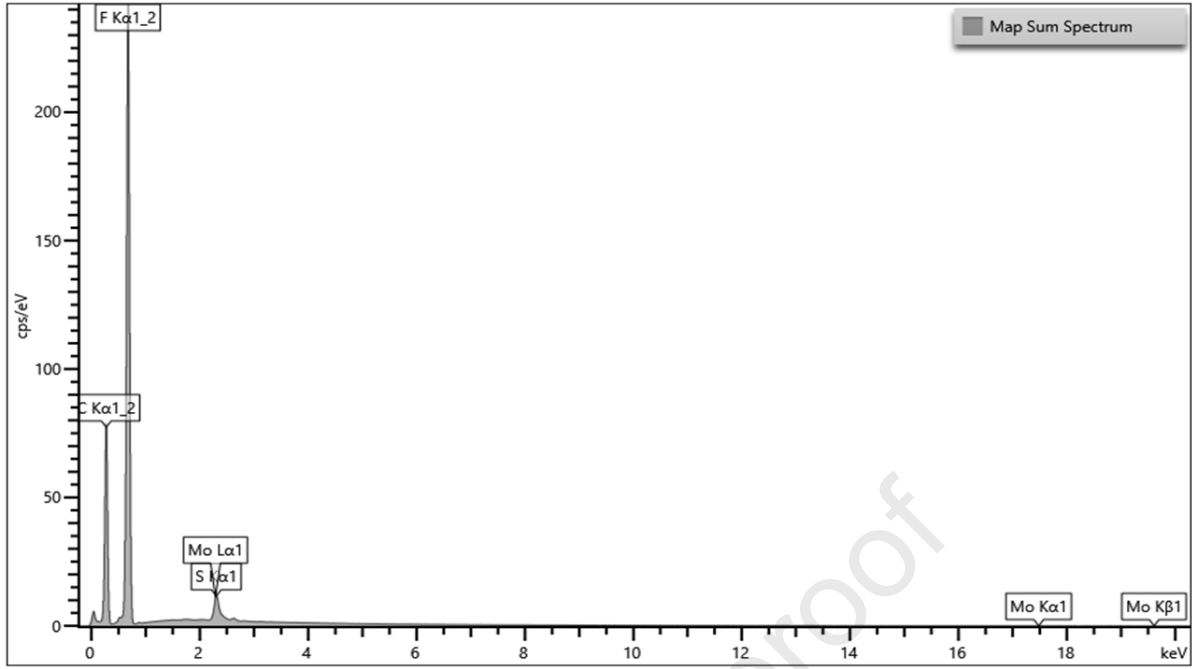


Figure S3: EDAX spectrum of MoS<sub>2</sub>-PVDF film surface showing relative concentration of MoS<sub>2</sub> in the PVDF matrix.

### Calculation of the piezoelectric coefficient $d_{33}$

The  $d_{33}$  value was calculated following the commonly used ‘dimensional model’ as reported by Katsouras et al. (ref. [34] in the main manuscript):

$$d_{33} = \left. \frac{\partial P_s}{\partial \sigma} \right|_{E=0} = \frac{\partial \left( \frac{\mu}{V} \right)}{\partial \sigma} = P_r \left( \frac{\partial \ln \mu}{\partial \sigma} - \frac{\partial \ln V}{\partial \sigma} \right) = P_r \left( \frac{\partial \ln \mu}{\partial \sigma} - \frac{1}{Y} \right) \approx -\frac{P_r}{Y} \quad (1)$$

where  $P_s$  is the spontaneous polarization due to macroscopic dipole moment  $\mu$ ,  $V$  is the sample volume,  $\sigma$  applied stress,  $P_r$  the remnant polarization and  $Y$  the Young’s modulus of the film.

Here the  $\frac{\partial \ln \mu}{\partial \sigma}$  is insignificant and is neglected assuming rigidity of the dipoles, and the compliance  $\frac{\partial \ln V}{\partial \sigma}$ , by definition, is  $(1/Y)$ , i.e. the inverse of Young’s modulus (see ref. [34] in the main manuscript).

Thus, according to this model and assumptions,  $d_{33}$  can be expressed as a ratio of  $P_r$  and  $Y$ . We determined  $P_r$  from P-E loop measurements and measured  $Y$  separately.

### Calculation for external force (F) on the MPNG

The applied force on the MPNG during finger tapping can be qualitatively estimated following momentum and energy conservation law:  $mgh = mv^2/2$ , i.e.,



$$v = (2gh)^{1/2} \quad (2)$$

$$(F - mg)\Delta t = mv \quad (3)$$

where  $m$ ,  $v$ ,  $h$  and  $F$  represent the mass of the impacting object, i.e. finger(s), velocity of the object when it touches the MPENG, falling height of the object and applied force, respectively. The symbol  $g$  denotes acceleration due to gravity and  $\Delta t$  is the time between two successive positive or negative peak of the voltage versus time graph.

In present work,  $m = 1.7$  kg,  $v = 1.384$  m/s,  $h = 0.15$  m (determined through video recording, see Video S1), and  $g = 9.8$  m/s<sup>2</sup>,  $\Delta t = 0.2167$  s. Thus, using equation (3), the force of the finger impacts on the MPNG is determined to be  $F = 27.5$  N which corresponds to a pressure of 64.5 kPa.

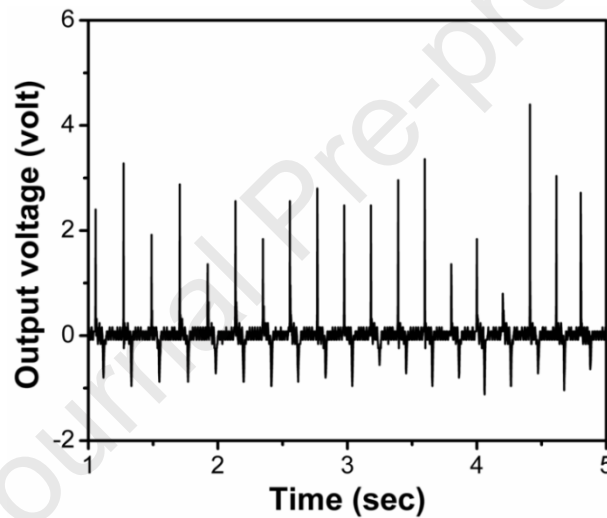


Figure S4: Open circuit output voltage of pure PVDF based nanogenerator under human finger tapping force which shows a weak output voltage due to some amount of piezoelectric phase developed during solution casting process.

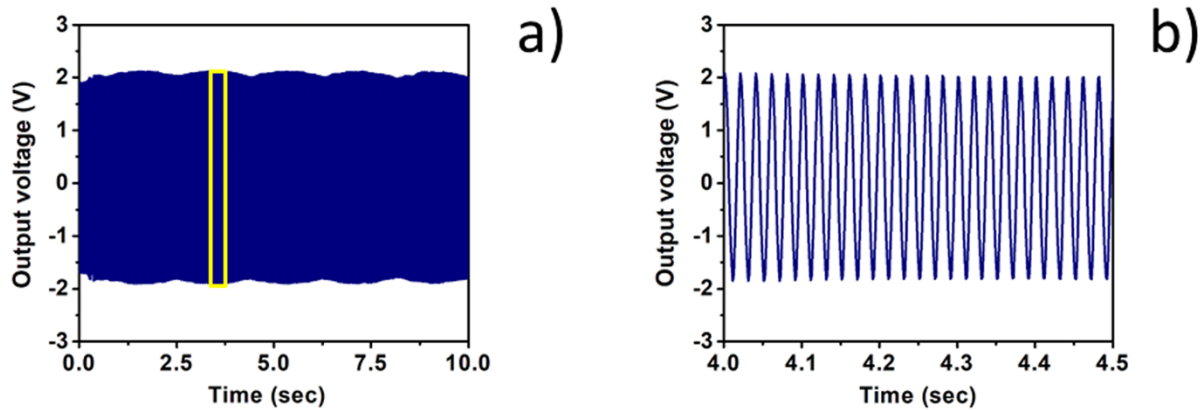


Figure S5: Open circuit output voltage of MPNG under a) ultrasonic vibration and b) magnified image from the selected region of a) (marked by yellow rectangle) showing individual peaks.

Table S1: Comparison of output voltage, current and power density of our MPNG with some previously reported nanogenerators based on PVDF nanocomposites. Our self-poled, MPNG device shows highest achievable performance under human finger tapping based on voltage output, current, power density and force applied.

Nanogenerator	Poling Status	Voltage (V)	Current (I)	Power Density	Pressure	Dimensions (Area $\times$ thickness)
PVDF/AlO-rGO <sup>[1]</sup>	Self-poled	36 V	0.8 $\mu$ A	27.97 $\mu$ W/cm <sup>3</sup>	36 kPa	7.82 cm <sup>2</sup> $\times$ 0.13 cm
rGO-Ag/PVDF <sup>[2]</sup>	Self-poled	18V	1.08 $\mu$ A	28 $\mu$ W/cm <sup>3</sup>	NA	22 cm <sup>2</sup> $\times$ N.A.
Fe-rGO/PVDF <sup>[3]</sup>	Self-poled	5.1V	0.254 $\mu$ A	N.A.	12 kPa	6 cm <sup>2</sup> $\times$ N.A.
ZnO NWs/PVDF <sup>[4]</sup>	100 kV/mm	0.2 V	10 nA	2 $\mu$ W/cm <sup>3</sup>	N.A.	N.A.
Nano ZnO/PVDF (0.2M ZnO loading) <sup>[5]</sup>	5 MV/m	4 V	N.A.	N.A.	4.4 kPa	0.25 cm <sup>2</sup> $\times$ 10 $\mu$ m
Cerium complex-PVDF <sup>[6]</sup>	Self-poled	36 V	N.A.	N.A.	N.A.	3.75 cm <sup>2</sup> $\times$ N.A.
$\gamma$ -PVDF/ZnO <sup>[7]</sup>	Self-poled	28 V	450 nA	0.4 $\mu$ W/cm <sup>3</sup>	8.43 kPa	7.2 cm <sup>2</sup> $\times$ N.A.
PVDF/DNA <sup>[8]</sup>	Self-poled	20 V	0.184 $\mu$ A	11 $\mu$ W/cm <sup>2</sup>	63 kPa	N.A.
BaTiO <sub>3</sub> -PVDF <sup>[9]</sup>	2 kV	35 V	600 nA	NA	1 MPa	1 cm <sup>2</sup> $\times$ N.A.
FAPbBr <sub>3</sub> -PVDF <sup>[10]</sup>	50 kV/cm	30 V	6.2 $\mu$ A	27.4 $\mu$ W/cm <sup>2</sup>	0.5 MPa	1.68 cm <sup>2</sup> $\times$ N.A.
PVDF/ 2D-MoS <sub>2</sub> <sup>[11]</sup>	10 kV	14V	N.A.	N. A.	8.8 kPa	N.A.

PVDF/few layer MoS <sub>2</sub> -cellulose <sup>[12]</sup>	18 kV	50 V	30 nA	N.A.	N.A.	9 cm <sup>2</sup> × N.A.
PVDF/ZnO ( <i>in situ</i> ) <sup>[13]</sup>	Self-poled	50 V	3.05 μA	32.8 mW/cm <sup>3</sup>	70 kPa	0.64 cm <sup>2</sup> × 20 μm
Niobate/PVDF <sup>[14]</sup>	Self-poled	18V	2.6 μA	N.A.	125 kPa	4 cm <sup>2</sup> × N.A.
<b>Present work</b>	<b>Self-poled</b>	<b>84V</b>	<b>2.8 μA</b>	<b>47.14 mW/cm<sup>3</sup></b>	<b>67.5 kPa</b>	<b>1 cm<sup>2</sup> × 50 μm</b>

Journal Pre-proof

Table S2: Comparison of capacitor charging ability of our MPNG with other PENGs reported earlier.

Nanogenerator	Capacitor ( $\mu\text{F}$ )	Time required (s)
PVDF/AlO-rGO <sup>[1]</sup>	2.2	96.6
Cerium complex-PVDF <sup>[6]</sup>	1	70
$\gamma$ -PVDF/ZnO <sup>[7]</sup>	1	100
PVDF/DNA film <sup>[8]</sup>	2.2	230
FAPbBr <sub>3</sub> -PVDF <sup>[10]</sup>	3.3	200
PVDF/ 2D-MoS <sub>2</sub> <sup>[11]</sup>	1	44
PVDF/ZnO ( <i>in situ</i> ) <sup>[13]</sup>	1	13
Yb <sup>3+</sup> / PVDF <sup>[15]</sup>	1	30
P(VDF-HFP)/Zn <sup>2+</sup> film <sup>[16]</sup>	1	70
<b>Present work</b>	<b>1</b>	<b>20</b>

#### Piezocatalytic effect of MoS<sub>2</sub>-PVDF

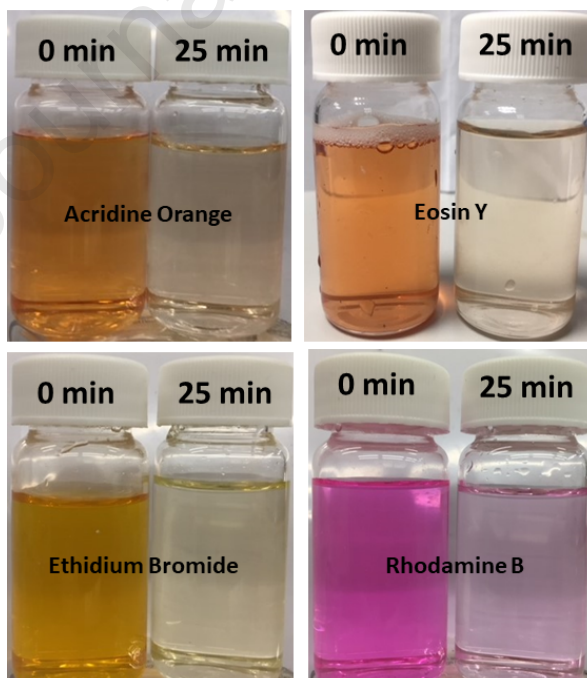


Figure S6: Piezocatalytic degradation of dyes as observed by relative decolorization after 25 minutes of ultrasonic vibration with PVDF-MoS<sub>2</sub> film.

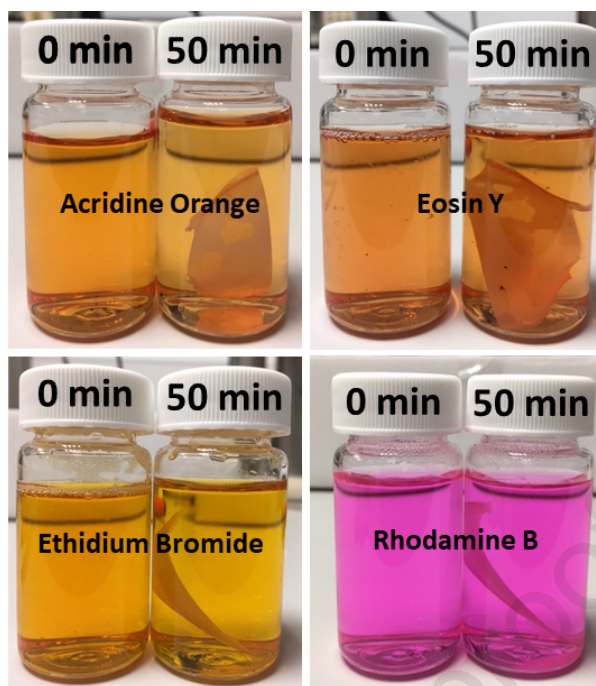


Figure S7: Assessing degradation of dyes by pure PVDF film (without any MoS<sub>2</sub>) under ultrasonic vibration. Clearly there is no dye degradation.

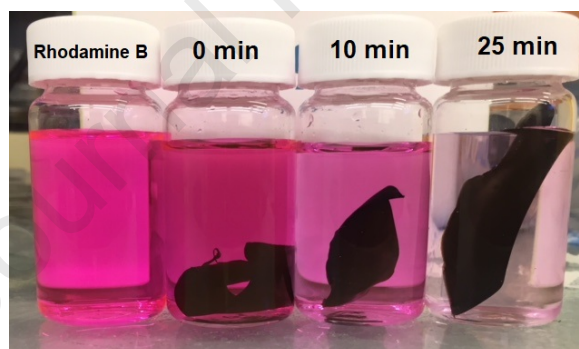


Figure S8: Time dependent piezocatalytic degradation of Rhodamine B by MoS<sub>2</sub>-PVDF films under ultrasonic vibration.

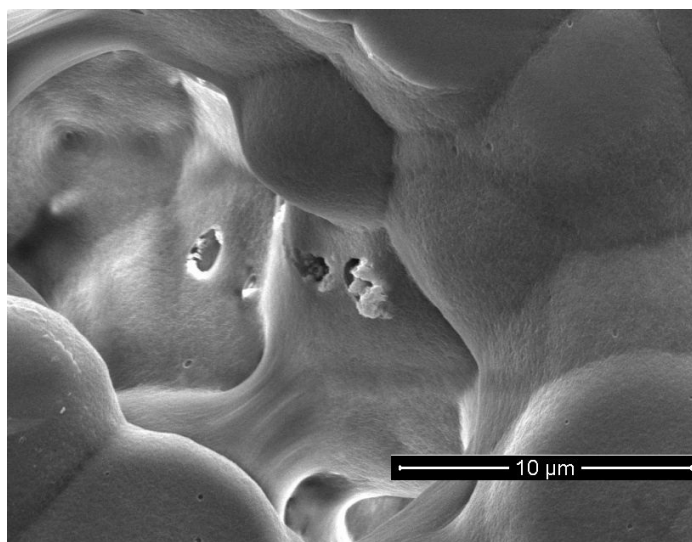


Figure S9: SEM micrograph of MoS<sub>2</sub>-PVDF film surface after 10 cycles of catalytic experiment showing negligible degradation of microstructure.

Video S1: Demonstration of lighting up commercially available blue LEDs using our MPNG under finger tapping.

Video S2: Demonstration of output voltage from the MPNG device under gentle finger tapping.

Video S3: Demonstration of maximum output voltage from the MPNG device under vigorous finger tapping.

Video S4: Demonstration of output voltage from the MPNG device under bending and twisting motion (showing negligible triboelectric effect).

#### References:

- [1] S. K. Karan, R. Bera, S. Paria, A. K. Das, S. Maiti, A. Maitra, B. B. Khatua, An approach to design highly durable piezoelectric nanogenerator based on self-poled PVDF/AlO-rGO flexible nanocomposite with high power density and energy conversion efficiency, *Adv. Energy Mater.* 6 (2016) 1601016-1601028.
- [2] L. Pusti, L. Sinha, P. M. Shirage, A flexible self-poled piezoelectric nanogenerator based on a rGO-Ag/PVDF nanocomposite, *New J. Chem.* 43(2019) 284-294.
- [3] S. K. Karan, D. Mandal, B. B. Khatua, Self-powered flexible Fe-doped RGO/PVDF nanocomposite: an excellent material for a piezoelectric energy harvester, *Nanoscale*, 7(2015)10655-10666.
- [4] M. Lee, C. Y. Chen, S. Wang, S. N. Cha, Y. J. Park, J. M. Kim, L. J. Chou, Z. L. Wang, A hybrid piezoelectric structure for wearable nanogenerators, *Adv. Mater.* 24(2012) 1759-1764.

- [5] R. Bhunia, S. Das, S. Dalui, S. Hussain, R. Paul, R. Bhar, A. K. Pal, Flexible nano-ZnO/polyvinylidene difluoride piezoelectric composite films as energy harvester, *Appl. Phys.* 122(2016) 637-650.
- [6] S. Garain, T. K. Sinha, P. Adhikary, K. Henkel, S. Sen, S. Ram, C. Sinha, D. Schmeiber, D. Mandal, Self-poled transparent and flexible UV light-emitting cerium complex-PVDF Composite: A high-performance nanogenerator, *ACS Appl. Mater. Interfaces* 7(2015)1298-1307.
- [7] S. Jana, S. Garain, S. K. Ghosh, S. Sen, D. Mandal, The preparation of  $\gamma$ -crystalline non-electrically poled photoluminescent ZnO-PVDF nanocomposite film for wearable nanogenerators, *Nanotechnology*, 27(2016)445403-445415.
- [8] A. Tamang, S. K. Ghosh, S. Garain, M. M. Alam, J. r. Haeberle, K. Henkel, D. Schmeisser, D. Mandal, DNA-assisted  $\beta$ -phase nucleation and alignment of molecular dipoles in PVDF Film: A realization of self-poled bioinspired flexible polymer nanogenerator for portable electronic devices, *ACS Appl. Mater. Interfaces*, 7(2015) 16143-16147.
- [9] Y. Zhao, Q. Liao, G. Zhang, Z. Zhang, Q. Liang, X. Liao, Y. Zhang, High output piezoelectric nanocomposite generators composed of oriented BaTiO<sub>3</sub> NPs@PVDF Nano Energy, 11(2015) 719-727.
- [10] R. Ding, X. Zhange, G. Chenc, H. Wangd, R. Kishorb, J. Xiaod, F. Gaob, K. Zengd, X. Chenc, X. W. Sune, Y. Zheng, High-performance piezoelectric nanogenerators composed of formamidinium lead halide perovskite nanoparticles and poly(vinylidene fluoride), *Nano Energy*, 37(2017) 126-135.
- [11] K. Maity, B. Mahanty, T. K. Sinha, S. Garain, A. Biswas, S. K. Ghosh, S. Manna, S. K. Ray, D. Mandal, Two-dimensional piezoelectric MoS<sub>2</sub>-modulated nanogenerator and nanosensor made of poly(vinylidene fluoride) nanofiber webs for self-powered electronics and robotics, *Energy Technol.* 5(2017) 234-243.
- [12] P. Sahatiya, S. Kannan, S. Badhulika, Few layer MoS<sub>2</sub> and in situ poled PVDF nanofibers on low cost paper substrate as high performance piezo-triboelectric hybrid nanogenerator: Energy harvesting from handwriting and human touch, *Appl Mater Today*, 13(2018)91-99.
- [13] P. Thakur, A. Kool, N. A. Hoque, B. Bagchi, F. Khatun, P. Biswas, D. Brahma, S. Roy, S. Banerjee, S. Das, Superior performances of in situ synthesized ZnO/PVDF thin film based self-poled piezoelectric nanogenerator and self-charged photo-power bank with high durability, *Nano Energy*, 44(2018) 456-467.
- [14] C. Zhang, Y. Fan, H. Li, Y. Li, L. Zhang, S. Cao, S. Kuang, Y. Zhao, A. Chen, G. Zhu, Z. L. Wang, Fully Rollable Lead-Free Poly(vinylidene fluoride)-Niobate-Based Nanogenerator with Ultra-Flexible Nano-Network Electrodes, *ACS Nano* 12 (2018) 4803-4811.

[15] S. K. Ghosh, A. Biswas, S. Sen, C. Das, K. Henkel, D. Schmeisser, D. Mandal, Yb<sup>3+</sup> assisted self-polarized PVDF based ferroelectric nanogenerator: A facile strategy of highly efficient mechanical energy harvester fabrication Nano Energy, 30(2016)621-629.

[16] P. Adhikary, D. Mandal, Enhanced electro-active phase in a luminescent P(VDF–HFP)/Zn<sup>2+</sup> flexible composite film for piezoelectric based energy harvesting applications and self-powered UV light detection, Phys.Chem.Chem.Phys. 19(2017)17789-17798.

Journal Pre-proof



## Highlights

- MoS<sub>2</sub> nanoflower embedded self-poled PVDF nanocomposite film is synthesized by simple solution casting.
- The nanocomposite film exhibited both piezoelectric and piezocatalytic activity.
- An impressive power density of 47.14 mW/cm<sup>-3</sup> has been achieved with the developed nanogenerator under human finger tapping.
- The film also showed high dye degradation capability (>90%) in dark condition under ultrasonic vibration due to piezocatalytic activity.

**Declaration of interests**

The authors declare that they have no known competing financial interests or personal relationships that could have appeared to influence the work reported in this paper.

The authors declare the following financial interests/personal relationships which may be considered as potential competing interests:

The corresponding author this manuscript is a director of an UCL spin out company (TCR Materials Ltd) which is trying to commercialize superhydrophobic materials. We do not perceive this to be a conflict.